catalysts

MDPI

Article

Synthesis and Structure of Copper Complexes of a N_6O_4 Macrocyclic Ligand and Catalytic Application in Alcohol Oxidation

Zhen Ma [1,2,*], Qijun Wang [1], Elisabete C. B. A. Alegria [2,3], M. Fátima C. Guedes da Silva [2,*], Luísa M. D. R. S. Martins [2], João P. Telo [2], Isabel Correia [2] and Armando J. L. Pombeiro [2,*]

1 School of Chemistry and Chemical Engineering, Guangxi University, Nanning 530004, China; dennis1992@live.cn

2 Centro de Química Estrutural, Complexo I, Instituto Superior Técnico, Universidade de Lisboa, Av. Rovisco Pais, 1049-001 Lisbon, Portugal; ebastos@deq.isel.ipl.pt (E.C.B.A.A.); luisamargaridamartins@tecnico.ulisboa.pt (L.M.D.R.S.M.); jptelo@itecnico.ulisboa.pt (J.P.T.); icorreia@tecnico.ulisboa.pt (I.C.)

3 Chemical Engineering Department, Instituto Superior de Engenharia de Lisboa, Instituto Politécnico de Lisboa, R. Conselheiro Emídio Navarro, 1959-007 Lisboa, Portugal

* Correspondence: mzmz2009@126.com (Z.M.); fatima.guedes@tecnico.ulisboa.pt (M.F.C.G.d.S.); pombeiro@tecnico.ulisboa.pt (A.J.L.P.); Tel.: +351-218-419-237 (A.J.L.P.)

Received: 9 April 2019; Accepted: 26 April 2019; Published: 7 May 2019

Abstract: Reactions between N_6O_4 macrocyclic 1,4,19,22,25,40-hexaaza-10,13,31,34-tetraoxa-6,14,27,35(1,4)-tetrabenzenacyclopentacontane (L) and several copper salts (*viz.* trifuoromethane and toluene sulfonates, nitrate, perchlorate, benzoate, and acetate) led to the formation of dinuclear compounds $[Cu_2(OSO_2CF_3)_2(DMF)_2L](SO_3CF_3)_2$ (**1**), $[Cu_2(p\text{-}OSO_2C_6H_4Me)_2L(DMF)_2](SO_3C_6H_4Me)_2$ (**2**), $[Cu_2(ONO_2)_2L(DMF)_2](NO_3)_2$ (**3**), $[Cu_2(OClO_3)_2(DMF)_2L](ClO_4)_2$ (**4**), $[Cu_2(OOCPh)_2L(H_2O)_2](O_2CPh)_2$ (**5**), and $[Cu_2(OOCMe)_4L]$ (**6**), which were characterized by IR, elemental analysis and TG-DTA (thermogravimetric-differential thermal analysis), as well as by single-crystal X-ray diffraction, EPR (electron paramagnetic resonance) spectroscopy, and electrochemical techniques (cyclic voltammetry and controlled potential electrolysis). The molecular structures of compounds **1**–**6** reveal a considerable conformational flexibility of the ligand L, which allowed its readjustment for the formation of the metal compounds and confirmed the presence of dinuclear *endo* macrocyclic species. In every case, the L ligand coordinates to each copper cation via three nitrogen atoms, with the remaining coordination positions of the metal square pyramid environment being accomplished by neutral or anionic ligands. The macrocyclic cavities appear to be adequate for the enclosure of a neutral species as proved by compound **6** with 1,4-dioxane. The compounds, in combination with the TEMPO (2,2,6,6-tetramethyl-piperidinyloxyl) radical and in alkaline aqueous solution, act as efficient catalysts in the aerobic oxidation of different alcohols to the corresponding aldehydes (yields up to 99% and TON up 232) after 20 h at 70 °C. In addition, the microwave-assisted solvent-free peroxidative oxidation (by *tert*-butylhydroperoxide, TBHP) of 1-phenylethanol led to acetophenone yields up to 99% and TOF of 1.1×10^3 after 0.5 h, without any additive.

Keywords: macrocyclic; copper complexes; catalysis; alcohol oxidation

1. Introduction

Much current attention has been paid to macrocyclic and macrobicyclic compounds due to their properties in selective complexation of metal cations, cation transport, and many other fields and in coordination, electrochemical, photoluminescent, catalytic, and biological chemistry [1–27].

Moreover, copper-containing compounds are of a high potential interest, because copper is a cheap and widespread metal in nature [28,29], the third most abundant essential trace metal in the human body, and present in the active sites of many enzymes [30–39], e.g., particulate methane monooxygenase, ceruloplasmin, haemocyanines, catechol oxidase, tyrosinase, and blue oxidases.

The oxidation of alcohols to carbonyl-containing compounds is one of the significant transformations of organic synthesis, because the resultant products are used in a variety of industries, continuing to attract increasing attention with the emergence of new catalysts, substrates, and oxidants [40]. The development of efficient greener oxidation systems using less poisonous and economic catalysts, oxidants, and solvents under mild conditions has become a relevant aim for catalysis. Among the numerous methods, oxidation of alcohols to corresponding carbonyl compounds by O_2, H_2O_2, or *t*-BuOOH, so called "green oxidants", still requires high temperatures and/or long times [40]. Thus, the development of new catalysts for the peroxidative oxidation of alcohols, operating under mild conditions, remains essential.

Copper(II) complexes with *N*,*N*- and *N*,*O*-ligands, in conjunction with the TEMPO (2,2,6,6-tetramethyl-piperidinyloxyl) radical, can be efficient catalysts for the selective oxidation of alcohols into corresponding carbonyl compounds [40]—a key reaction that is widely used in organic synthesis.

Continuing our research devoted to the preparation of copper complexes with N-based ligands constructed from polyaza species, including terpyridine, macrocyclic, and/or macrobicyclic compounds, and study of their structural, electrochemical, catalytic, and biological properties [41], we now report the synthesis, characterization, and catalytic application of six new copper compounds, constructed from reactions of a series of copper salts with the macrocyclic species 1,4,19,22,25,40-hexaaza-10,13,31,34-tetraoxa-6,14,27,35(1,4)-tetrabenzenacyclopentacontane (L, Scheme 1), *viz.*: $[Cu_2(OSO_2CF_3)_2(DMF)_2L](SO_3CF_3)_2$ (**1**), $[Cu_2(p\text{-}OSO_2C_6H_4Me)_2L(DMF)_2](SO_3C_6H_4Me)_2$ (**2**), $[Cu_2(ONO_2)_2L(DMF)_2](NO_3)_2$ (**3**), $[Cu_2(OClO_3)_2(DMF)_2L](ClO_4)_2$ (**4**), $[Cu_2(OOCPh)_2L(H_2O)_2](O_2CPh)_2$ (**5**), and $[Cu_2(OOCMe)_4L]$ (**6**). The compounds were characterized by IR, elemental analysis, TGA, electrochemical techniques (cyclic voltammetry and controlled potential electrolysis), EPR (electron paramagnetic resonance), and by single-crystal X-ray diffraction. The catalytic properties of the compounds towards the aerobic oxidation of alcohols were investigated and the influence of various parameters, such as reaction time, type of catalyst, temperature, and presence of additives, was evaluated.

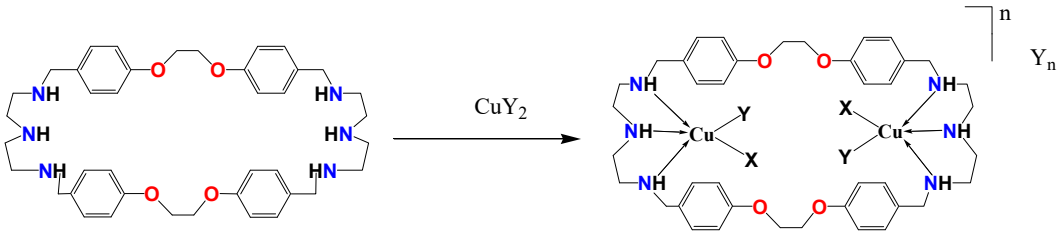

Scheme 1. General procedure for the synthesis of the dicopper(II) macrocyclic compounds [n = 2+, X = DMF, Y = OSO_2CF_3 (**1**); X = DMF, Y = $OSO_2C_6H_4Me$ (**2**); X = DMF, Y = ONO_2 (**3**); X = DMF, Y = $OClO_3$ (**4**); X = H_2O, Y = OCOPh (**5**); n = 0, X = Y = OCOMe (**6**)].

2. Results and Discussion

The macrocyclic ligand L was obtained by hydrogenation of the Schiff-base macrocyclic compound 1,4,19,22,25,40-hexaaza-10,13,31,34-tetraoxa-6,14,27,35(1,4)-tetrabenzena

cyclotriacontaphane-5,18,26,39-tetraene with KBH_4, and it was then allowed to react with the appropriate Cu(II) salt (Scheme 1 and Experimental section), *viz.* $Cu(SO_3CF_3)_2{\cdot}2H_2O$, $Cu(p\text{-}SO_3PhCH_3)_2{\cdot}4H_2O{\cdot}CH_3OH$, $Cu(NO_3)_2{\cdot}2.5H_2O$, $Cu(ClO_4)_2{\cdot}6H_2O$, $Cu(CO_2Ph)_2$, or $Cu(CO_2Me)_2{\cdot}H_2O$, leading to the formation of the Cu(II) compounds $[Cu_2(OSO_2CF_3)_2(DMF)_2L](SO_3CF_3)_2$ (**1**), $[Cu_2(p\text{-}OSO_2C_6H_4Me)_2L(DMF)_2](SO_3C_6H_4Me)_2$ (**2**), $[Cu_2(ONO_2)_2L(DMF)_2](NO_3)_2$ (**3**), $[Cu_2(OClO_3)_2(DMF)_2L](ClO_4)_2$ (**4**), $[Cu_2(OOCPh)_2L(H_2O)_2](O_2CPh)_2$ (**5**), and $[Cu_2(OOCMe)_4L]$ (**6**), in this order. The reactions usually proceeded smoothly at room temperature, and the compounds were isolated after 24 h in good to high yields (39%–79%). They were obtained as blue solids and were characterized (see Experimental and Supporting Information) by X-ray diffraction, elemental, IR, and thermogravimetric-differential thermal analysis (TG-DTA), as well as by cyclic voltammetry (CV) and controlled potential electrolysis (CPE).

In the IR spectrum of L, the very strong band at 3420 cm^{-1} conceivably includes the ν(N–H) of the compound and ν(O–H) of both methanol and of H_2O; the ν(C=C) band occurs between 1611 and 1515 cm^{-1}. In the compounds, while the N–H stretching vibration of the ligand L is shifted towards lower wavenumbers appearing at 3244 (in **1**), 3190 (in **2**), 3200 (in **3**), 3240 (in **4**), 3219 (in **5**), or 3239 cm^{-1} (in **6**), the ν(C=C) bands occur at values similar to those found in the free L species. The counter ions in compounds **1**–**5** show their typical ν(S=O) or ν(C=O) bands at 1658 (in **1**), 1652 (in **2**), 1652 (in **3**), 1656 (in **4**), and 1665 cm^{-1} (in **5**).

The electronic spectra of compounds **1**–**6** exhibit two or three absorption bands in the 222–285 nm range assigned to ligand-to-metal charge transfers (LMCT); a less intense absorption band occurs between 603 and 619 nm and is due to $d \rightarrow d$ transitions. The effect of a basic solution was tested for compound **6**, but no significant change was detected in the positions of the bands, although a change in their intensities occurs.

Conductivity measurements were performed for all compounds. The molar conductivity values suggest 1:2 electrolytes for compounds **1**–**5** and a non-electrolyte for compound **6**, in accord with the proposed formulation established by X-ray diffraction. The increase in conductivity in the basic solution of compound **6** is due to the high concentration of ionic species in solution.

2.1. X-Ray Diffraction Analysis

X-ray quality single crystals of the compounds were obtained upon recrystallization from dimethylformamide (DMF)/diethyl ether (for **1**–**4**) or evaporation of a solution of methanol/1,4-dioxane mixture (for **5**, **6**). The crystallographic data are summarized in Table 1, and a comparison of selected dimensions is presented in Table 2.

Table 1. Crystallographic data for compounds **1**–**6**.

	1·0.5H$_2$O	**2·2DMF·2H$_2$O**	**3·6DMF·0.5CH$_4$O**	**4·2H$_2$O**	**5·C$_4$H$_8$O$_2$·2H$_2$O**	**6·C$_4$H$_8$O$_2$·5H$_2$O**
empirical formula	$C_{50}H_{69}Cu_2F_{12}N_8O_{18.5}S_4$	$C_{80}H_{114}Cu_2N_{10}O_{22}S_4$	$C_{64.5}H_{106}Cu_2N_{18}O_{24.5}$	$C_{46}H_{72}Cl_4Cu_2N_8O_{24}$	$C_{72}H_{90}Cu_2N_6O_{18}$	$C_{52}H_{84}Cu_2N_6O_{19}$
fw	1561.51	1823.13	1652.77	1390.00	1454.60	1224.35
cryst syst	Triclinic	Triclinic	Triclinic	Monoclinic	Triclinic	Triclinic
T (K)	120	150	120	150	298	150
Space group	$P\,\bar{1}$	$P\,\bar{1}$	$P\,\bar{1}$	$P21/n$	$P\,\bar{1}$	$P\,\bar{1}$
a (Å)	10.832(2)	13.0363(19)	12.9020(6)	17.7983(6)	9.1949(18)	9.5711(19)
b (Å)	12.331(3)	13.801(2)	13.3540(6)	8.9329(3)	11.473(2)	9.823(2)
c (Å)	13.336(3)	14.449(3)	14.4500(8)	18.9816(6)	18.881(4)	18.144(4)
α (deg)	79.37(3)	100.354(8)	109.270(5)	90	73.07(3)	78.20(3)
β (deg)	70.16(3)	99.297(8)	95.630(4)	95.854(2)	78.86(3)	79.53(3)
$\gamma\gamma$ (deg)	85.05(3)	116.479(8)	112.130(5)	90	80.88(3)	61.04(3)
V (Å^3)	1646.3(6)	2201.0(6)	2105.41(18)	3002.15(17)	1858.5(6)	1454.2(5)
Z	1	1	1	2	1	1
D_{calc} (Mg m^{-3})	1.575	1.375	1.304	1.538	1.300	1.398
μ (Mo Kα) (mm^{-1})	0.880	0.654	0.585	0.971	0.643	0.808
Independent reflections	5801	11065	7615	5220	9219	6338
Observed reflections	5239	8164	6375	2934	7292	5381
R_{int}	0.0223	0.0368	0.0310	0.0539	0.0208	0.0241
R [a]	0.0733	0.0453	0.0780	0.0736	0.0555	0.0364
wR [b]	0.1828	0.1278	0.2239	0.1839	0.1632	0.0921

[a] $R = \Sigma||F_o| - |F_c||/\Sigma|F_o|$. [b] $wR = [\Sigma[w(F_o^2 - F_c^2)^2]/\Sigma[w(F_o^2)^2]]^{1/2}$.

Table 2. Selected bond distances (Å) and angles (°) for compounds **1–6**.

	1	**2**	**3**	**4**	**5**	**6**
τ_5[50]	0.03	0.08	0.04	0.03	0.15	0.15
d(Cu^{2+}) relative to l.s. basal plane	−0.1785(18)	−0.2043(3)	0.6311(14)	−0.2457(11)	0.1671(11)	−0.1898(3)
Cu–$O_{equatorial}$	1.955(3)	1.9703(15)	1.979(2)	1.927(4)	1.9561(19)	1.9461(18)
Cu–O_{axial}	2.275(3)	2.2518(17)	2.240(3)	2.352(5)	2.264(2)	2.211(2)
	2.000(4)	1.9942(19)	1.997(4)	1.986(6)	2.004(2)	2.002(2)
Cu–N	2.024(3)	2.0470(18)	2.040(3)	2.011(5)	2.044(2)	2.025(2)
	2.036(3)	2.0729(18)	2.042(4)	2.031(5)	2.046(2)	2.032 (2)
∠ N2–Cu–N3	168.07(14)	163.46(8)	165.69	163.5(2)	164.30	163.01(8)
Intramolecular Cu···Cu	12.518(5)	10.888(2)	11.032(1)	10.990 (2)	12.019 (4)	11.941 (4)
Largest intramolecular N···N	15.858(9) Å	14.215(5)	14.350(6)	14.42(1)	12.246(6)	11.316(5)
Chirality at N2, N3 ($N2^i$, $N3^i$)	SR(RS)	RS(SR)	SR(RS)	SR(RS)	RR(SS)	RR(SS)

In every structure of the compounds (Figures 1–6) an inversion center is sited at the heart of the macrocyclic cavity; one half of each molecule and one metal cation are present in the asymmetric units, and the other halves being generated by symmetry. The macrocyclic L ligand chelates to the two copper cations by means of the six N atoms (three for every cation), thus leading to two fused five-membered CuNCCN metallacycles; the copper coordination spheres are then fulfilled with one *O*-DMF and either one *O*-trifluoromethane sulfonate (in compound **1**), one *O*-toluenesulfonate (in compound **2**), one nitrate (in compound **3**) or one perchlorate (in compound **4**), one benzoate anion and one water molecule (compound **5**), or two acetate anions (in **6**), giving rise to N_3O_2 square pyramidal geometries (τ_5 parameter values [42] in the 0.03–0.15 range; Table 2). Among the compounds, only **6** is neutral, with the charges of **1–5** being balanced by the same anionic species present in the coordination spheres of the metals.

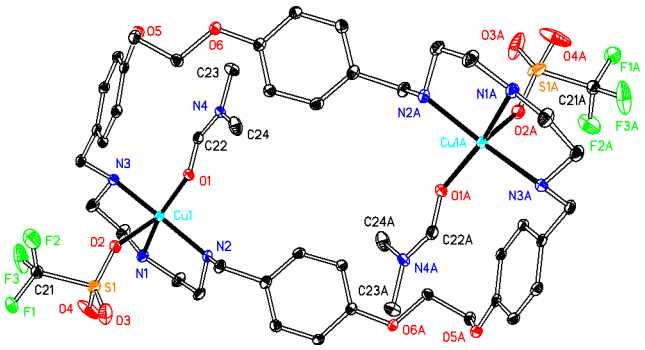

Figure 1. Molecular structure of the $[Cu_2(OSO_2CF_3)_2L(DMF)_2]^{2+}$ complex cation of compound **1** with atom labeling scheme; the two trifluoromethane sulfonate anions and the water molecules were omitted for clarity. Ellipsoids are drawn at 30% probability. Symmetry operation to generate equivalent atoms: *A*) 2-x,1-y,-z. Selected bond lengths (Å) and angles (°): Cu1-N1 2.000(4), Cu1-N2 2.024(3), Cu1-N3 2.036(3), Cu1-O1 1.955(3), Cu1-O2 2.275(3); N1-Cu1-N2 84.72(15), N1-Cu1-N3 85.84(14), N2-Cu1-N3 168.07(14), O1-Cu1-N1 166.16(14), O1-Cu1-N2 88.00(13), O1-Cu1-N3 99.67(13), O1-Cu1-O2 99.21(12), N1-Cu1-O2 93.14(14), N2-Cu1-O2 94.87(13), and N3-Cu1-O2 92.92(13).

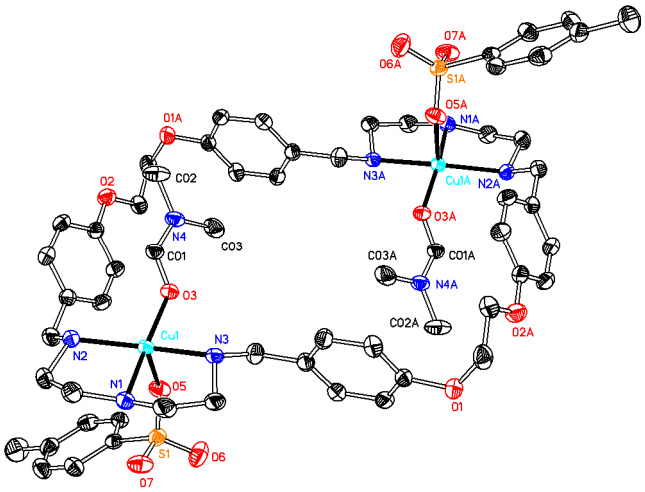

Figure 2. Molecular structure of the $[Cu_2$-*p*-$(OSO_2C_6H_4CH_3)_2L(DMF)_2]^{2+}$ complex cation of compound **2** with atom labeling scheme; the two *p*-toluenesulfonate anions, dimethylformamide (DMF), and water molecules, including hydrogen atoms were omitted for clarity. Ellipsoids are drawn at 50% probability. Symmetry operation to generate equivalent atoms: *A*) 1-x,1-y,-z. Selected bond lengths (Å) and angles (°): Cu1-N1 1.9951(19), Cu1-N2 2.0727(18), Cu1-N3 2.0465(18), Cu1-O3 1.9703(15), Cu1-O5 2.2517(18); N1-Cu1-N2 84.71(8), N1-Cu1-N3 83.86(8), N1-Cu1-O5 98.63(8), N2-Cu1-O5 97.12(7), N3-Cu1-N2 163.47(8), N3-Cu1-O5 96.36(7), O3-Cu1-N1 168.30(7), O3-Cu1-N3 89.44(7), O3-Cu1-N2 99.68(7), O3-Cu1-O5 91.62(7).

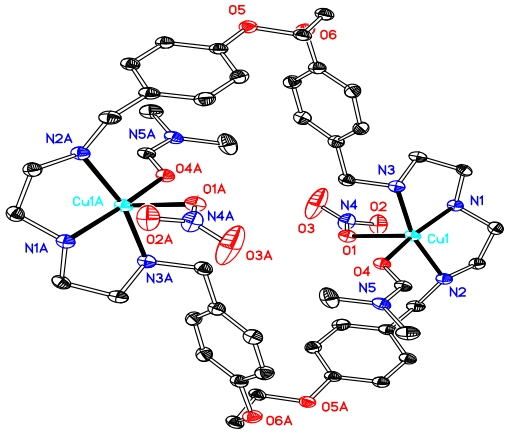

Figure 3. Molecular structure of the $[Cu_2(NO_3)_2(DMF)_2L]^{2+}$ complex cation of compound **3** with atom labeling scheme; the DMF and water molecules were omitted for clarity. Ellipsoids are drawn at 30% probability. Symmetry operation to generate equivalent atoms: *A*) -x, 2-y, 1-z. Selected bond lengths (Å) and angles (°): Cu1-N1 1.997(4), Cu1-N2 2.042(4), Cu1-N3 2.031(4), Cu1-O1 2.240(3), Cu1-O4 1.979(3);O4-Cu1-N1 163.20(14), O4-Cu1-N3 89.15(13), N1-Cu1-N3 84.98(14), O4-Cu1-N2 97.97(13), N1-Cu1-N2 84.70(14), N3-Cu1-N2 165.69(16), O4-Cu1-O1 90.63(12), N1-Cu1-O1 105.36(13), N3-Cu1-O1 93.00(14), N2-Cu1-O1 99.28(14), N4-O1-Cu1 120.0(3).

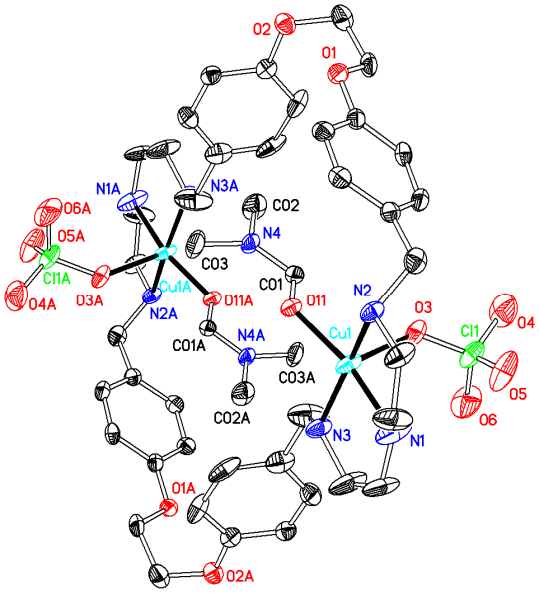

Figure 4. Molecular structure of the $[Cu_2(ClO_4)_2(DMF)_2L]^{2+}$ complex cation of compound **4** with atom labeling scheme; the perchlorate anions and the water molecules were omitted for clarity. Ellipsoids are drawn at 30% probability. Symmetry operation to generate equivalent atoms: *i*) 1-x,2-y,1-z. Selected bond lengths (Å) and angles (°): Cu1-N1 1.985(6), C1-N2 2.031(5), Cu1-N3 2.011(5), Cu1-O3 2.352 (5), Cu1-O11 1.927(4); O11-Cu1-N1 165.7(3), O11-Cu1-N3 93.45(19), N1-Cu1-N3 85.0(2), O11-Cu1-N293.25(18), N1-Cu1-N2 84.8(2), N3-Cu1-N2 163.6(2), O11-Cu1-O3 91.21(17), N1-Cu1-O3 103.1(3), N3-Cu1-O3 91.8(2), N2-Cu1-O3 103.1(2).

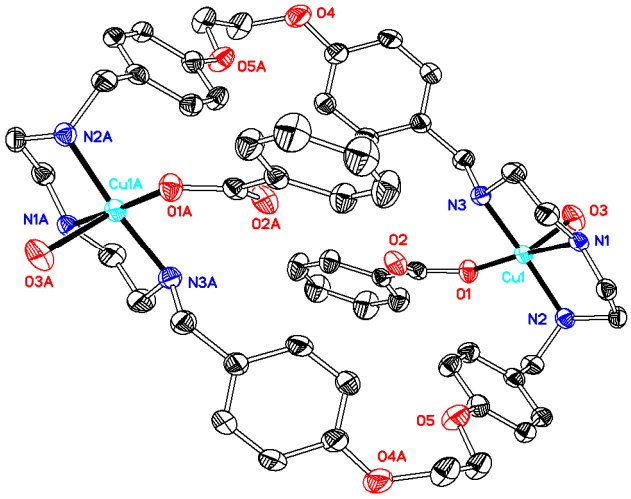

Figure 5. Molecular structure of the $[Cu_2(CO_2Ph)_2L(H_2O)_2]^{2+}$ complex cation of compound **5** with atom labeling scheme; the dioxane and water molecules were omitted for clarity. Ellipsoids are drawn at 30% probability. Symmetry operation to generate equivalent atoms: *A*) 2-x,-y,-z. Selected bond lengths (Å) and angles (°): Cu1-N1 2.004(2), Cu1-N2 2.044(2), Cu1-N3 2.046(2), Cu1-O1 1.9561(19), Cu1-O3 2.264(2); O(1)-Cu(1)-N(1) 173.23(9), O1-Cu1-N2 92.45(9), N1-Cu1-N2 85.49(10), O1-Cu1-N3 96.45(9), N1-Cu1-N3 84.17(9), N2-Cu1-N3 164.30(9), O1-Cu1-O3 91.00(9), N1-Cu1-O3 95.55(9), N2-Cu1-O3 93.25(10), N3-Cu1-O3 99.48(10).

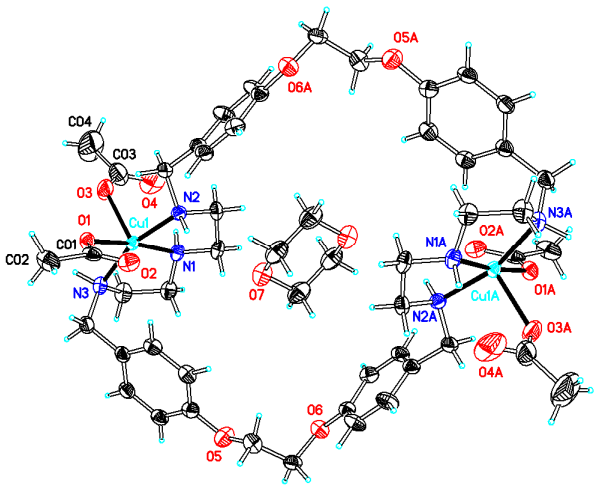

Figure 6. Molecular structure of the $[Cu_2(CO_2CH_3)_4L]$ dioxane aggregate of compound **6** with atom labeling scheme; the water molecules were omitted for clarity. Ellipsoids are drawn at 30% probability. Symmetry operation to generate equivalent atoms: *i*) 1-x,2-y,-z. Selected bond lengths (Å) and angles (°): Cu1-N1 2.002(2), Cu1-N2 2.032(2), Cu1-N3 2.025(2), Cu1-O1 1.9461(18), Cu1-O3 2.211(2); N1-Cu1-N2 84.89(8), N1-Cu1-N3 85.45(8), N3-Cu1-N2 163.01(8), O1-Cu1-N1 172.23(8), O1-Cu1-N3 90.68(8), O1-Cu1-N2 97.17(8), O1-Cu1-O3 91.22(9), N1-Cu1-O3 95.85(9), N2-Cu1-O3 99.28(8), N3-Cu1-O3 95.57(9).

The hydrophobic internal environments of compounds **1**–**6** are able to encapsulate neutral molecules, as proven by compound **6** which trapped a 1,4-dioxane molecule. To corroborate this statement, it was shown that the DMF co-ligands in compounds **1**–**4** are leaning towards the center of the macrocycle; however, in compound **5** both co-ligands (the anionic acetate and the neutral water) are facing the exterior of the ring.

The axial Cu–O bond distances (in the 2.211(2)–2.352(5) Å range, Table 2) are longer than the equatorial ones (between 1.927(4) and 1.979(2) Å), with the differences in each compound assuming values that vary between 0.261 and 0.425 Å; the longest $Cu–O_{equatorial}$ bond was found in compound **3**, while compound **1** presents the longest $Cu–O_{axial}$. It is compound **4** that presents the shortest Cu–N value (1.986(6) Å, Table 2) and compound **2** the longest one (2.0729(18) Å). The largest Cu···Cu and N···N intramolecular distances were found in compound **1**.

Compound **1** shows intermolecular π–π interactions (*centroid*···*centroid* distances of 3.659 Å) between neighboring aryl groups of the L ligand (see Figure S1). The structure also revealed intermolecular C–H···π interactions (C···*centroid* distance of 3.471 Å) as well as F···π contacts (F···*centroid* of 4.593 Å), both involving the same C15> C20 aromatic ring. Medium/weak intramolecular hydrogen bonds involve the N–H or C–H groups (as donors) and the $O_{sulfonate}$ or O_{DMF} moieties (as acceptors) in the 2.755–3.223 Å range.

In the remaining compounds, several O···π or H···π interactions are found. The structures of compounds **2** and of **3** show C_{DMF}–H···π interactions with C···*centroid* distances of 3.811 and of 3.625 Å, respectively (Figures S12 and S13, respectively). In compounds **4**–**6**, the $O_{perchlorate}$, $O_{benzoate}$, or $O_{acetate}$ coligands interact intramolecularly with the delocalized electron density of the Cu-N-C-C-N metallacycles [3.761 (compound **4**), 3.711 (compound **5**), or 3.627–3.780 Å (compound **6**), Figures S4–S6).

2.2. Electrochemical Behavior

The electrochemical behaviors of compounds **1**–**6** were investigated by cyclic voltammetry (CV) and controlled potential electrolysis (CPE) at a platinum working electrode at 25 °C in a 0.2 M $[^nBu_4N][BF_4]$/DMSO solution. A typical cyclic voltammogram is shown in Figure 7.

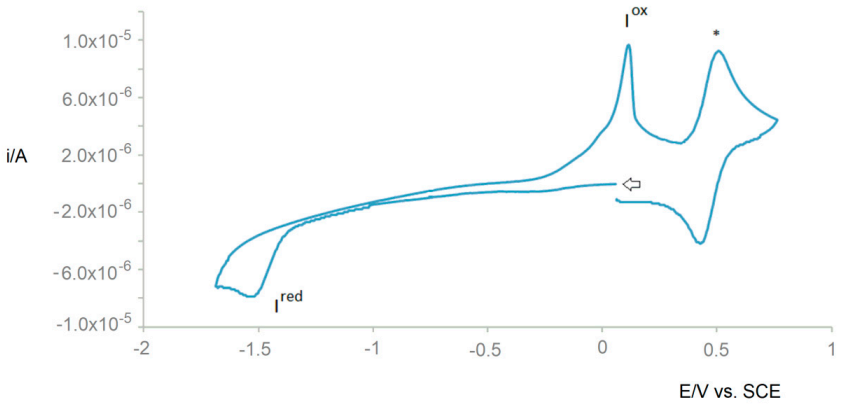

Figure 7. Cyclic voltammogram, initiated by the cathodic sweep, of compound **3** in a 0.2 M [^{n}Bu$_4$N][BF$_4$]/DMSO solution, at a Pt disc working electrode (d = 0.5 mm), run at a scan rate of 200 mVs^{-1}. * [Fe(η^5-C$_5$H$_5$)$_2$]$^{0/+}$.

Complexes **1**–**6** exhibit, per Cu center, one two-electron (as measured by CPE) irreversible reduction wave at $^{red}E_p$ peak potential values (Table 3) in the −1.44 to −1.87 V vs. SCE (saturated calomel electrode) range, assigned to the Cu(II) → Cu(0) reduction (wave **I^{red}**). The lowest reduction potential ($^{red}E_p$ = −1.87 V vs. SCE) is observed for the neutral complex **6**, which is thus harder to reduce than the cationic complexes (**1**–**5**), as expected. No Cu–Cu interaction was detected by CV, on account of the distance between the copper ions.

No anodic waves were detected for any of the complexes. However, upon scan reversal, after the cathodic process, an irreversible (with desorption) anodic wave (**I^{ox}**) at −0.10 to 0.24 V vs. SCE (Table 3, Figures 7 and 8) was observed, corresponding to the oxidation of cathodically generated deposited metallic copper [43].

Table 3. Cyclic voltammetric data [a] for compounds **1**–**6**.

Compound	$^{red}E_p$ (I^{red})	$^{ox}E_p$ (I^{ox}) [b]
1	−1.78	−0.11
2	−1.67	−0.01
3	−1.53	0.10
4	−1.44	0.24
5	−1.60	−0.02
6	−1.87	−0.05

[a] Potential values in Volt ± 0.02 vs. SCE, in a 0.2 M [^{n}Bu$_4$N][BF$_4$]/DMSO solution, at a Pt disc working electrode determined by using the [Fe(η^5-C$_5$H$_5$)$_2$]$^{0/+}$ redox couple ($E_{1/2}{}^{ox}$ = 0.44 V vs. SCE[41,48]) as the internal standard at a scan rate of 200 mVs^{-1}. [b] Anodic wave generated upon scan reversal following the reduction wave.

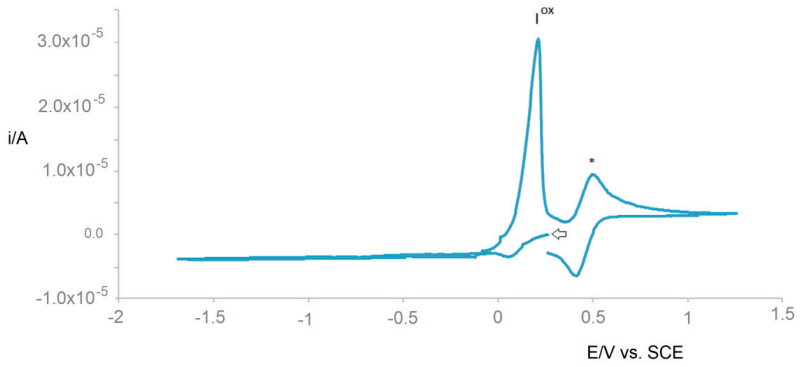

Figure 8. Cyclic voltammogram, initiated by the cathodic sweep, after controlled potential electrolysis (CPE) at the reduction wave (I^{red}) of compound **3**, in a 0.2 M [^{n}Bu$_4$N][BF$_4$]/DMSO solution, at a Pt disc working electrode (d = 0.5 mm), 200 mVs^{-1}. * [Fe(η^5-C$_5$H$_5$)$_2$]$^{0/+}$.

2.3. EPR Characterization

The EPR spectra of the compounds were measured in DMF (compounds **1**–**3**) or in a 0.85:0.15 dichloromethane/methanol solvent mixture (compounds **5** and **6**) at 100 K (Figure 9). Table 4 presents the optimized sets of spin Hamiltonian parameters obtained by simulation. Figures S7–S10 show the experimental and simulated EPR spectra for the compounds.

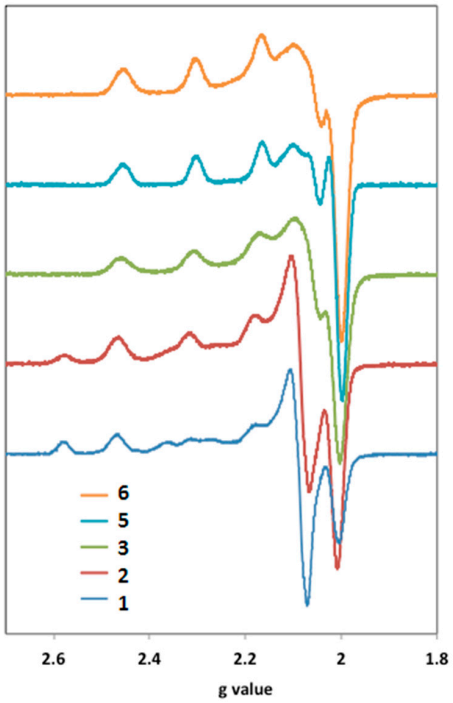

Figure 9. X-band EPR spectra of compounds **1**–**3** (in DMF) and of compounds **5** and **6** [in dichloromethane (85%)/methanol(15%) solvent mixtures] measured at 100 K.

Table 4. Spin Hamiltonian parameters of the compounds obtained by simulation.

Compound	g_x	g_y	g_z	A_x [$\times 10^{-4}$cm^{-1}]	A_y [$\times 10^{-4}$cm^{-1}]	A_z [$\times 10^{-4}$cm^{-1}]	%	g_z/A_z [$\times 10^{-4}$cm]
1	2.082	2.082	2.410	0.0	0.0	132.8	55	181.5
	2.042	2.069	2.242	29.2	26.9	181.1	44	123.8
2	2.080	2.080	2.410	0.0	0.0	132.8	31	181.5
	2.042	2.070	2.243	29.2	26.9	181.2	68	123.8
3	2.033	2.063	2.239	24.1	34.3	180.8	100	123.8
5	2.032	2.060	2.229	24.0	33.6	183.9	100	121.2
6	2.032	2.060	2.230	22.4	35.8	181.4	100	122.9

The complexes show well-resolved hyperfine structures, and most of the spectra were simulated considering rhombic symmetry for *g* and *A* tensors. All spectra are characterized by having $g_z > g_{x,y}$, indicating that the unpaired electron occupies the $d_{x2\text{-}y2}$ ground state, which is typical of octahedral, square pyramid, or square planar geometries. This orbital points directly towards the equatorial ligands and consequently can couple magnetically with the nuclear spin of ^{14}N donor atoms. This is known in coordination chemistry as superhyperfine coupling. Due to line broadening, it was not possible to detect this kind of superhyperfine structure in the compounds of this study.

For complexes **3**, **5**, and **6**, only one copper species is present, and because the linewidths are well fitted with a Gaussian descriptor, no dipolar coupling occurs; thus, the two copper centers are equivalent and far apart. For compounds **1** and **2**, two distinct species appear to be present in the batches used for this EPR analysis: one corresponds to the respective macrocyclic complex and the other

to a solvated copper ion [44], whose spectrum was simulated considering axial tensors. The parameters obtained for the Cu(II)-macrocyclic species are similar for all compounds (Table 4), suggesting identical binding sets.

The g_z/A_z ratio has been used as an empirical indicator known as the tetrahedral distortion index [45]; the larger its value, the greater the extent of the tetrahedral distortion. Values within the range from 100×10^{-4} to 135×10^{-4} cm indicate octahedral, square based pyramidal, or square planar geometries. For compounds **1**–**3**, **5,** and **6,** the values are within this range, suggesting minimal tetrahedral distortions and supporting the square pyramidal geometries established by X-ray diffraction (see above). The results also confirm that only one of the X,Y co-ligands (Scheme 1) is in the equatorial plane, the other being in the axial position and weakly coordinated.

2.4. Thermal Properties

Except for compound **4**, which is expected to be explosive at high temperature due to the perchlorate counter ion, the thermal properties of the other five compounds **1**–**3**, **5**, and **6** were studied, and selected results are shown in the Supplementary Materials (Table S1; Figures S12–S16).

For instance, the decomposition process of compound **1** (Figure S12) has three major steps of weight losses in its TG and DTA curves. The first one is until ca. 200 °C with a weight loss of 1.9%, complying to the weight loss of solvents. The second process occurs up to 430 °C with 52.3% weight loss and corresponds to the loss of two $N(C_2H_4)_2$ and four SO_3CF_3 groups (calc. 51.4%). The next loss of 4.30 mg in weight (33.7%) occurs until 575 °C, corresponds to the loss of CH_2PhO groups, and is followed by the decomposition of the leftover of the compound leading to CuO with a residual weight of 11.8% of the starting complex, which is identical to the calculated value of 11.1%.

The TG and DTA curves for compound **2** (Figure S13) also indicate three major weight losses. The first one, up to 150 °C, is attributed to the evolution of the DMF and the water molecules, whether coordinated or not, with a total weight loss of solvents of 17.7%. The second decomposition step evolves from 250 to 450 °C with a total weight loss of 32.1% and corresponds to the loss of two $N(C_2H_4)_2$ and of the SO_3 and CH_3 groups (calc. 31.4%). The third step runs up to 720 °C, shows a weight loss of 39.6% and is assigned to the decomposition of the leftover of the compound, giving CuO as the final product with a residual weight of 10.3% (calc. 8.7%).

Details for the other complexes are presented in Table S1 and Figures S14–S16, Supplementary Materials.

2.5. Catalytic Behavior of Compounds **1**–**6**

Aerobic oxidation of benzylic alcohols. The copper(II) complexes **1**–**6** have been tested as catalysts (0.0075 mmol, 0.5 mol% based on substrate) for the aerobic oxidation of benzylic alcohols (1.5 mmol) in alkaline (1 M K_2CO_3) aqueous solution and in the presence of the TEMPO radical (0.075 mmol, 5 mol% based on substrate), to the corresponding aldehydes (Scheme 2) under previously established reaction conditions (70 °C, 6 or 20 h, 1 atm air) [46]. For comparative purposes, cinnamyl alcohol and 1-phenylethanol were also used as substrates under similar reaction conditions. All the complexes were shown to be much more active than the precursor salts, proving the promoting effect of ligands in the metal-assisted steps of this catalytic oxidation reaction. However, the ligand itself was not able to catalyze the benzyl alcohol to oxidation of benzaldehyde under the same reaction conditions. The selected results are shown in Table 5.

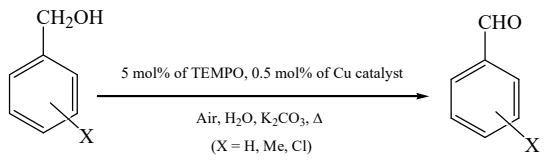

Scheme 2. Aerobic oxidation of benzylic alcohols in aqueous solution.

Table 5. Aerobic oxidation of benzyl alcohols to the corresponding carbonyl compounds catalyzed by **1–6** [a].

Entry	Complex	Substrate	Product	Time (h)	Yield [b] (%)	TON [TOF(h^{-1})] [c]
1 [d]	-	benzyl alcohol	benzaldehyde	20	5	10 (1)
2 [e]	L	benzyl alcohol	benzaldehyde	20	4	9 (1)
3	**1**	benzyl alcohol	benzaldehyde	20	97	197 (10)
4	**2**	benzyl alcohol	benzaldehyde	20	99	201 (10)
5	**3**	benzyl alcohol	benzaldehyde	20	94	191 (10)
6	**4**	benzyl alcohol	benzaldehyde	20	79	160 (8)
7	**5**	benzyl alcohol	benzaldehyde	20	84	168 (8)
8	**6**	benzyl alcohol	benzaldehyde	20	99	232 (12)
9 [f]	**6**	benzyl alcohol	benzaldehyde	20	7	14 (1)
10 [g]	**6**	benzyl alcohol	benzaldehyde	20	27	55 (3)
11	**6**	benzyl alcohol	benzaldehyde	6	54	110 (18)
12	**6**	benzyl alcohol	benzaldehyde	9	64	130 (14)
13 [h]	**6**	benzyl alcohol	benzaldehyde	20	3	9 (1)
14 [i]	**6**	benzyl alcohol	benzaldehyde	20	26	53 (3)
15 [j]	**6**	benzyl alcohol	benzaldehyde	20	86	166 (8)
16	**6**	2-Me-benzyl alcohol	2-Me-benzaldehyde	20	64	129 (14)
17	**6**	4-Me-benzyl alcohol	4-Me-benzaldehyde	20	88	171 (9)
18	**6**	2-Cl-benzyl alcohol	2-Cl benzaldehyde	20	72	146 (7)
19	**6**	4-Cl-benzyl alcohol	4-Cl-benzaldehyde	20	91	185 (9)
20	**6**	cinnamyl alcohol	cinnamaldehyde	20	57	108 (5)
21	**6**	1-phenylethanol	acetophenone	20	63	126 (6)

[a] Conditions, unless stated otherwise: 1.5 mmol of substrate, 0.0075 mmol of Cu catalyst (0.5 mol% based on substrate), 0.075 mmol of TEMPO (5 mol% based on substrate) in aqueous solution of K_2CO_3 (5 mL, 1 M), 70 °C, 1 atm air. [b] Molar yield (%) based on substrate, i.e., moles of product per 100 moles of substrate, determined by GC. [c] TON = turnover number = number of moles of product per mol of metal catalyst; TOF = TON per hour (values in brackets). [d] Without catalyst. [e] In the presence of the macrocyclic ligand (L). [f] Using just water instead of the basic aqueous solution. [g] Without TEMPO. [h] 30 °C. [i] 50 °C. [j] 90 °C.

Complexes **1–3** and **6** are the most active catalysts under the conditions of this study, resulting in 94%–99% yields in benzaldehyde after 20 h of reaction of benzyl alcohol at 70 °C (Table 5, entries 3–5 and 8). The formation of the corresponding carboxylic acid was not observed (GC-MS) conceivably on account of the propensity of TEMPO for scavenging free radicals, acting as an effective radical trap, avoiding the auto-oxidation of aldehydes [47,48]. TEMPO is a known promoter in alcohol oxidation catalysis [47,49] and it was confirmed to be crucial in our system. In fact, the reaction performed in its absence resulted in a benzaldehyde yield lowering, e.g., from 99% to 27% for compound **6** (Table 5, compare entries 8 and 10). The presence of base (K_2CO_3) is also relevant, as expected: carrying out the reaction with **6** as a catalyst and in the absence of the base results in a drastic yield reduction from 99% to 7% (Table 5, compare entries 8 and 9).

Performing the aerobic oxidation of benzyl alcohol in the presence of compound **6** (one of the most active catalysts) at temperatures lower than 70 °C resulted in yield reduction (Figure 10 and Table 5, entries 13 and 14). For temperatures higher than that value, the observed yield decrease conceivably results from the lower solubility of dioxygen in the reaction solution (Figure 10 and Table 5, entry 15).

The dependence of the product yield on the reaction time also with **6** as the catalyst is illustrated in Figure 11. Despite the modest yield of 54% after the first 6 h, a good value of 86% was observed after 12 h, and 97% was reached after 16 h, which is close to the almost quantitative value after 20 h (Table 5, entry 8).

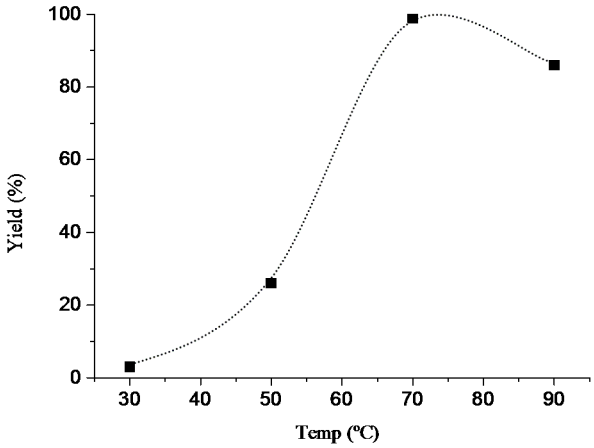

Figure 10. Effect of the temperature on benzaldehyde yield (mol% vs. substrate) in the aerobic oxidation of benzyl alcohol, catalyzed by compound **6**. Reaction conditions: substrate (1.5 mmol), 0.0075 mmol of Cu catalyst and 0.075 mmol of TEMPO in 5 mL of 1 M K_2CO_3 aqueous solution for 20 h.

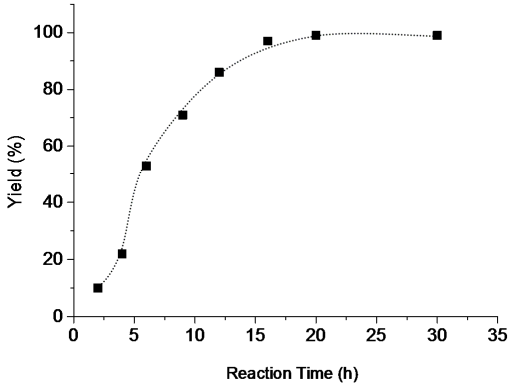

Figure 11. Dependence of benzaldehyde yield on the reaction time, catalyzed by compound **6**. Reaction conditions: substrate (1.5 mmol), 0.0075 mmol of Cu catalyst and 0.075 mmol of TEMPO in 5 mL of 1 M K_2CO_3 aqueous solution.

Compound **6** can also catalyze the oxidation of benzylic alcohols into the corresponding aldehydes in good or moderate yields, which are in line with other reported Cu/TEMPO catalytic systems [40,46,50]. The oxidation of 2- and 4-methylbenzyl alcohol results in 64% and 88% yield of the corresponding aldehydes (Table 5, entries 16 and 17, respectively), while the chloro analogues are converted to 2- and 4-chlorobenzaldehyde in better yields (72% and 91%, Table 5, entries 18 and 19, respectively). The lower yields for the *ortho* substituted benzyl alcohols in comparison with the corresponding *para* compounds, together with the lower yields for the benzyl alcohols with electron-donor substituents relative to those with electron-attractor ones, reveal the expected both steric and electronic influences of the substituent (Table 5, entries 16–19).

The reaction, in the presence of **6** as the catalyst, is less effective for the oxidation of cinnamyl alcohol (57% yield, Table 5, entry 20), as previously reported for other Cu(II) complexes [46]. However, the secondary alcohol 1-phenylethanol is converted to the corresponding ketone (acetophenone), in a good yield (63%, Table 5, entry 21), in contrast with other much less effective Cu/TEMPO systems [40,51]. In any case, a lower yield is associated with the oxidation of the secondary alcohol in comparison with the primary benzyl alcohols, in accordance with the higher steric effects in the former and the lack (also in the former) of H-bond stabilization of the $PhHC^{\bullet}\text{-}O^{-}$ ligand (which occurs in the case of a benzyl alcohol, see below) upon interaction with coordinated TEMPO [47,52,53]. The use of *t*-BuOOH as oxidant under microwave irradiation (see below) leads to a marked higher acetophenone yield.

Recycling capacity is one of the important parameters for any catalyst, and therefore, complex 6 has been tested in up to 5 consecutive cycles for the aerobic oxidation of benzyl alcohol. A moderate reduction (10%) in product yield was observed after the second cycle, but in the following cycles, more pronounced values were obtained (up to 40% after the fifth cycle), suggesting deactivation of the active species during the catalytic reaction (or during the washing steps).

Our catalytic systems are expected [40,49–54] to involve the coordination (with deprotonation) of benzyl alcohol ($PhCH_2OH$) and of the TEMPO radical to the copper center, followed by hydrogen abstraction from the former by the latter with resulting formation of the *O*-ligated radical $PhHC^{\bullet}$-O^{-} and TEMPOH. Intramolecular electron-transfer from ligated $PhHC^{\bullet}$-O^{-} to Cu^{II} leads to the formation of the aldehyde PhCHO and Cu^{I}, which is re-oxidized to Cu^{II} by dioxygen (Scheme 3). The TEMPO radical is also regenerated upon oxidation of TEMPOH by dioxygen.

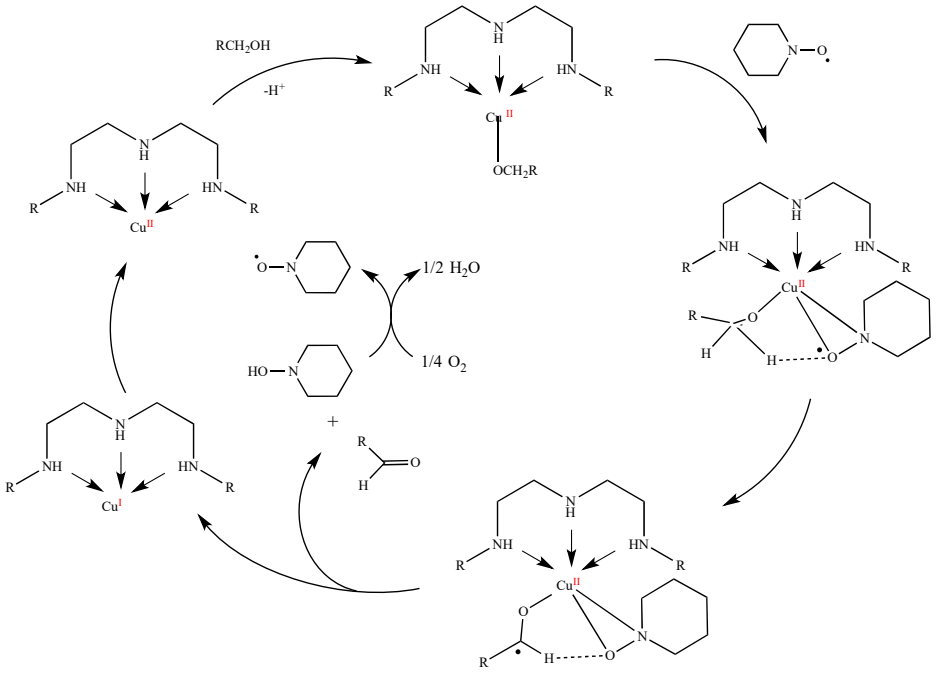

Scheme 3. Proposed mechanism for the aerobic oxidation of benzylic alcohols in aqueous solution and in the presence of TEMPO.

Solvent-free microwave (MW)-assisted oxidation of 1-phenylethanol. As mentioned above, the aerobic oxidation of 1-phenylethanol, used as a model substrate for secondary alcohols, leads, as expected, to a lower aldehyde yield than in the case of the primary benzyl alcohols. However, the catalytic oxidation of 1-phenylethanol can be highly promoted by using microwave irradiation following a previously developed procedure [55] with *tert*-butyl hydroperoxide (*t*-BuOOH) as the oxidizing agent. Typical reaction conditions concern 2 equivalent of *t*-BuOOH at 80 or 120 °C, under low power (5 or 15 W) microwave (MW) irradiation, 0.5 s 6 h reaction time and in the absence of any added solvent (Scheme 4, Table 6). Acetophenone is the only oxidation product detected. Under these conditions, much higher acetophenone yields can be achieved (see below and Table 6) than when using the conditions for the aerobic oxidation of 1-phenylethanol (see above and Table 5, entry 21). In fact, complexes **1**–**6** catalyze this reaction and lead to acetophenone yields up to 99% and TON of 542 (Table 6, entry 6 for catalyst **6**) for a Cu catalyst/substrate molar ratio of 0.2%, after 0.5 h reaction time at 120 °C without any additive.

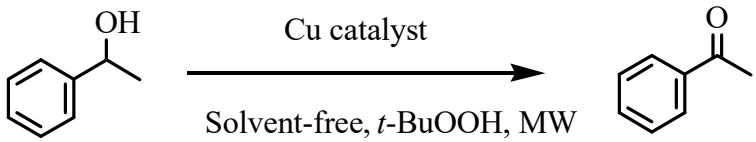

Scheme 4. Microwave (MW)-assisted solvent-free oxidation of 1-phenylethanol to acetophenone, with *t*-BuOOH.

Table 6. MW-assisted solvent-free peroxidative (with *t*-BuOOH) oxidation of 1-phenylethanol to acetophenone, catalyzed by compounds **1**–**6** [a].

Entry	Catalyst Precursor	Reaction Time (h)	Temperature (°C)	Additive (μmol)	Yield [b] (%)	TON [TOF(h^{-1})] [c]
1	**1**	0.5	120	-	79	390 (780)
2	**2**	0.5	120	-	66	326 (652)
3	**3**	0.5	120	-	81	412 (824)
4	**4**	0.5	120	-	64	302 (604)
5	**5**	0.5	120	-	68	325 (650)
6	**6**	0.5	120	-	99	542 (1.1×10^3)
7	**2**	0.5	80	-	13	114 (228)
8	**2**	6	80	-	26	256 (43)
9 [d]	**2**	0.5	80	-	42	105 (210)
10	**2**	0.5	120	TEMPO (30)	99	496 (992)
11	**6**	0.5	80	-	29	283 (566)
12	**6**	6	80	-	97	1.1×10^3 (182)
13	**6**	0.5	80	TEMPO (30)	49	249 (498)

[a] Reaction conditions (unless stated otherwise): 2.5 mmol of substrate, 5 μmol of Cu catalyst (0.2 mol% based on substrate), 5 mmol of *t*-BuOOH (aq. 70%), microwave irradiation (5 W at 80 °C and 15 W at 120 °C). [b] Molar yield (%) based on substrate, i.e., moles of product per 100 moles of substrate, determined by GC. [c] TON = turnover number = number of moles of product per mol of metal catalyst; TOF = TON per hour (values in brackets). [d] Amount of catalyst **2**: 10 μmol (0.4 mol% based on substrate).

Lowering the temperature slows down the reaction and, e.g., for compound **6** at 80 °C, only a 29% yield is observed after 0.5 h (Table 6, entry 11), which is much lower than the almost quantitative one at 120 °C (Table 6, entry 6). Such a behavior is similar to those observed in other cases [40,56,57].

We have also investigated the influence of TEMPO under MW irradiation in the catalytic oxidation of 1-phenylethanol with *t*-BuOOH. A marked promotion of the acetophenone yield occurs as in other reported cases [40,58] and, e.g., when compound **2** is used as the catalyst for 0.5 h of reaction time at 120 °C, a yield of 99% is achieved, while in the absence of the additive only 66% was obtained (entry 10 vs. entry 2, Table 6).

The possible mechanism can involve the generation of *t*-BuOO$^\bullet$ and *t*-BuO$^\bullet$ radicals, formed upon metal-assisted oxidation and reduction of *t*-BuOOH (Equations (1) and (2), respectively) [53,59], which behave as H-atom abstractors from the alcohol (Equations (4) and (5)) [59,60].

$$M^{(n+1)+} + t\text{-BuOOH} \rightarrow M^{n+} + t\text{-BuOO}^\bullet + H^+ \quad (1)$$

$$M^{n+} + t\text{-BuOOH} \rightarrow M^{(n+1)+}\text{-}(OH^-) + t\text{-BuO}^\bullet \quad (2)$$

$$M^{(n+1)+}\text{-}(OH^-) + t\text{-BuOOH} \rightarrow M^{(n+1)+}\text{-}(OO\text{-}\ t\text{-Bu}^-) + H_2O \quad (3)$$

$$t\text{-BuO}^\bullet + R_2CHOH \rightarrow t\text{-BuOH} + R_2C^\bullet\text{-OH} \quad (4)$$

$$t\text{-BuOO}^\bullet + R_2CHOH \rightarrow t\text{-BuOOH} + R_2C^\bullet\text{-OH} \quad (5)$$

$$M^{(n+1)+}\text{-}(OO\text{-}\ t\text{-Bu}^-) + R_2C^\bullet\text{-OH} \rightarrow R_2C{=}O + t\text{-BuOOH} + M^{n+} \quad (6)$$

3. Materials and Methods

All manipulations were performed under normal conditions, and the solvents were dried when necessary, by refluxing over the appropriate drying reagents and distilling under nitrogen prior to use. Elemental analyses were determined with an Elementar Vario EL III Elemental Analyzer (Elementar AnalysensystemeGmbH, Germany). Infrared spectra (4000–400 cm^{-1}) were recorded on a Jasco FT/IR-430 instrument (Jasco, Tokyo, Japan) in KBr pellets; wavenumbers are in cm^{-1}; abbreviations: vs, very strong; s, strong; m, medium; w, weak. ^{1}H and ^{13}C NMR spectra were run on a Varian Unity 400 spectrometer (Varian, USA) at ambient temperature. TG-DTA data were collected with a Perkin Elmer STA6000 Thermal Analyzer (Perkin-Elmer, Waltham, MA, USA) at a heating rate of 10 K min^{-1} under an air atmosphere. The EPR spectra were obtained at 100 K on a CW X-band Bruker ESP 300E Spectrometer (Bruker, Bremen, Germany). The X-band EPR spectra were analyzed using a program developed by Rockenbauer and Korecz [61]. The EPR spectra for compounds **1** and **2** were simulated by a superposition of two component curves. The fitting was achieved assuming either axial or rhombic *g* and *A* tensors. The electrical conductivity measurements (Λ_M, reported as S cm^2 mol^{-1}) of solutions of the copper compounds **1–6** (ca. 1.5×10^{-3} M) were taken with a WTW Multi 340 conductometer at 15 °C. The UV–Vis absorption spectra of dichloromethane/methanol or DMF solutions of **1–6** (ca. 1.5×10^{-3} M) in 1.00 cm quartz cells were recorded at room temperature on a Lambda 35 UV–Vis spectrophotometer (Perkin-Elmer) by scanning the 200–800 nm region at a rate of 240 nm min^{-1}. Reactions under microwave irradiation were performed by using a focused Anton Paar Monowave 300 reactor (Anton Paar GmbH, Graz, Austria).

3.1. Crystal Structure Determinations

The X-ray quality single crystals of compounds **1–6** were mounted in a Nylon loop or on glass fibers and measured at a temperature of 120 K (compounds **1**,**3**), 150 K (compounds **2**, **4,** and **6**), or 298 K (compound **5**). Intensity data were collected using an Agilent SuperNova (Dual, Atlas, compounds **1**, **3**, and **5**) or Bruker AXS-KAPPA APEX II (**2**, **4**, and **6**) diffractometers with graphite monochromated Mo-Kα (λ = 0.71073 Å) radiation. Data were collected using omega scans of 0.5° per frame, and a full sphere of data were obtained. For the former, cell parameters were retrieved using Agilent CrysAlisPro [62] software and refined using Agilent CrysAlisPro (Agilent Technologies, Oxfordshire, UK) [62] on all the observed reflections. For the latter, cell parameters were retrieved using Bruker SMART software and refined using Bruker SAINT (Bruker, Bremen, Germany) [63] on all the observed reflections. Absorption corrections were applied using SADABS [64]. Structures were solved by direct methods by using the SHELXS–97 package [65] and refined with SHELXL–97 [65]. Calculations were performed using the WinGX System–Version 1.80.03 [66]. All hydrogen atoms were inserted in calculated positions and constrained to ride on their parent atoms: C–H = 0.93–0.96|Å and N–H = 0.86|Å, with U_{iso}(H) = 1.5U_{eq}(C-methyl) and 1.2U_{eq}(C,N) for the other H atoms. Least square refinements were employed with anisotropic thermal motion parameters for all the non-hydrogen atoms and isotropic for the remaining atoms. The oxygen atoms at $SO_3CF_3^-$ as a coordinated auxiliary ligand and oxygen and fluorine atoms at the other counter ion in compound **1** are disordered. The occupancy factors of the disordered atoms were calculated automatically by Shelx-XL software and adjusted reasonably to two $SO_3CF_3^-$ counter ions totally. CCDC 846593, 846595, 1404617, 1404618, 1404619, and 1404620 contain the supplementary crystallographic data for this paper. These data can be obtained free of charge from the Cambridge Crystallographic Data Centre via www.ccdc.cam.ac.uk/data_request/cif.

3.2. Electrochemical Studies

The electrochemical experiments were performed on an EG&G PAR 273A potentiostat/galvanostat connected to a personal computer through a GPIB interface. Cyclic voltammograms (CV) were obtained in 0.2 M [^{n}Bu$_4$N][BF_4]/DMSO, at a platinum disc working electrode (*d* = 0.5 mm). Controlled-potential electrolyzes (CPE) were carried out in a three-electrode H-type cell and monitored regularly by

cyclic voltammetry. The compartments were separated by a sintered glass frit and equipped with platinum gauze working and counter electrodes. For both CV and CPE experiments, a Luggin capillary connected to a silver wire pseudo-reference electrode was used to control the working electrode potential. The solutions were bubbled with N_2 before each run. The redox potentials of the complexes were measured by CV in the presence of ferrocene (internal standard) relatively to the SCE by using the $[Fe(\eta^5\text{-}C_5H_5)_2]^{0/+}$ redox couple ($E^{OX}_{1/2}$ = 0.44 V vs. SCE in DMSO) [41,67].

3.3. Catalytic Studies

The aerobic oxidations of benzylic alcohols, cinnamyl alcohol, and 1-phenylethanol were typically performed in flasks fitted with water circulating condensers and under air at atmospheric pressure. 1.5 mmol of the substrate, 0.0075 mmol (0.5 mol% based on substrate) of Cu catalyst **1**–**6**, 0.075 mmol (5 mol%) of TEMPO and 5 mL of 1 M K_2CO_3 aqueous solution were added, and the reaction mixture was stirred for 20 h at 70 °C after which the additions of 0.5 mL of HCl 1 M (for neutralization) and 5 mL of EtOAc (for the extraction of the substrate and of the organic products from the reaction mixture) were accomplished. Then, 120 μL of cycloheptanone was added as internal standard, and the products were analyzed and quantified by GC (the internal standard method).

The MW-assisted solvent-free peroxidative oxidation experiments of 1-phenyethanol were performed using a 10 mL capacity reaction tube (13 mm Ø), fitted with a rotational system and an IR temperature detector. The alcohol (2.5 mmol), 5 μmol of Cu catalyst **1**–**6** (0.2 mol% based on substrate) and a 70% aqueous solution of *t*-BuOOH (5 mmol) were introduced in a sealed cylindrical Pyrex tube. The system was left under stirring and under irradiation of 5 W at 80 °C or 15 W at 120 °C for 0.5 h. After cooling to room temperature, 150 μL of benzaldehyde (internal standard) and 2.5 mL of MeCN (for substrate and organic products extraction) were added. After stirring for 10 min, a sample (1 μL) was taken from the organic phase and analyzed by GC.

Oxidation products were analyzed by gas chromatography using a FISONS Instruments GC 8000 series gas chromatograph with a flame ionization detector (FID) and a capillary column (DB-WAX, column length: 30 m; Ø: 0.32 mm) (He as the carrier gas) and the Jasco-Borwin v.1.50 software. The temperature of injection was 240 °C. The initial temperature of the column was kept at 120 °C for 1 min, elevated 10 °C/min up to 200 °C, and finally held at this temperature for 1 min. The attribution of peaks was made by comparison with commercial samples (GC) and, in some cases, by GC-MS analyses using a Perkin Elmer Clarus 600 C instrument (He as the carrier gas), equipped with a 30 m × 0.22 mm × 25 μm BPX5 (SGE) capillary column.

Synthesis of L. Compound L was synthesized by hydrogenation, with KBH_4, of the Schiff-base 1,4,19,22,25,40-hexaaza-10,13,31,34-tetraoxa-6,14,27,35(1,4)-tetrabenzenacyclotria contaphane-5,18,26,39-tetraene [68]. Then, 1.0 g (1.5 mmol) of this precursor and 400 mL of methanol were mixed in a 1000 mL flask, and a white emulsion was obtained. Next, 2.0 g (37 mmol) of KBH_4 were added in portions of 400 mg every 20 min. The colorless solution thus obtained was stirred for half an hour, filtered, and the solution taken to dryness. Upon the addition of 200 mL of water, it was left stirring for 1 h. Compound L was obtained as a white solid, which was isolated by filtration, recrystallized from methanol, and dried under vacuum (0.90 g, yield 89%), m.p. 177–179 °C. Anal. calcd for $C_{40}H_{54}N_6O_4{\cdot}CH_3OH{\cdot}2.5H_2O$ ($C_{41}H_{63}N_6O_{7.5}$; *mw* 759.97) C, 64.80; H, 8.36; N, 11.06. Found C, 64.87; H, 8.47; N, 10.82; ^{1}H NMR (400 MHz, CD_3OD: $CDCl_3$ = 1:4), δ 2.55 (s, 16H, NH–C*H*$_2$), 3.50 (s, 8H, C*H*$_2$ Ar), 4.09 (s, 8H, O–C*H*$_2$), 6.69 (d, *J* = 8.4 Hz, 8H, aryl), 7.00 (d, *J* = 8.4 Hz, 8H, aryl). ^{13}C NMR (100 MHz, CD_3OD: $CDCl_3$ = 1:4), δ 47.59 (CH_2-N), 47.68 (CH_2N), 52.59 (CH_2CH_2N), 66.41 (O-CH_2); 114.32 (aryl), 129.24 (aryl), 131.86 (aryl), 157.61 (aryl). IR (KBr disc) (cm^{-1}): 3420 (vs, $\nu_{O\text{-}H}$ and $\nu_{N\text{-}H}$), 2932 (s), 2832 (s), 1611 (s, $\nu_{aryl\text{-}H}$), 1515 (s), 1453 (s, $\nu_{aryl\text{-}H}$), 1380 (w), 1299 (m), 1243 (vs), 1180 (m), 1113 (m), 1068 (s), 939 (s), 810 (s), 770 (m), 616 (w), 522 (w).

Synthesis of $[Cu_2(OSO_2CF_3)_2L(DMF)_2](SO_3CF_3)_2$ (compound 1) $Cu(SO_3CF_3)_2{\cdot}2H_2O$ (0.29 g, 0.72 mmol) was dissolved in 10 mL of methanol, a solution of $L{\cdot}CH_3OH{\cdot}2.5H_2O$ (0.25 g, 0.33 mmol) in 20 mL mixture of methanol and dichloromethane (1:1) was added, and the system was stirred for

24 h. After filtration, the blue filtrate was taken to dryness, and 20 mL of diethyl ether was added, thus affording a blue solid. TG-DTA: CuO% = 11.8, weight% (for loss of solvents) = 1.9. Calcd with the formula of $C_{44}H_{54}Cu_2F_{12}N_6O_{16}S_4 \cdot 1.5H_2O$: CuO% = 11.1, weight% (for loss of H_2O) = 1.9. After dissolution of the compound in 20 mL of DMF and diffusion of diethyl ether through this solution, dark blue crystals were obtained, suitable for X-ray diffraction. Different batches of the compound were used for microanalysis and single-crystal X-ray diffraction. Total amount obtained: 0.20 g (39% yield based on L). Anal. calcd for $C_{44}H_{54}Cu_2F_{12}N_6O_{16}S_4 \cdot 2C_3H_7NO \cdot 4H_2O$ ($C_{50}H_{76}Cu_2F_{12}N_8O_{22}S_4$; *mw* 1624.52): C 36.97; H 4.72; N 6.90. Found: C 37.10; H 4.51; N 6.62. IR (KBr disc) (cm^{-1}): 3466 (vs), 3223 (s), 2946 (m), 2908 (s), 1658 (vs), 1612 (s, $\nu_{aryl\text{-}H}$), 1586 (w), 1513 (s, $\nu_{aryl\text{-}H}$), 1444 (s), 1384 (s), 1252 (vs), 1166 (vs), 1110 (s), 1100 (m), 1049 (vs), 926 (m), 821 (m), 765 (m), 701 (w), 652 (s), 578 (m), 521 (m). UV–Vis $_{max}$ in DCM/MeOH, nm (ε, $M^{-1}cm^{-1}$): 616 (35), 273 (401). Λ_M in DCM/MeOH: 110 Scm^2mol^{-1}.

Synthesis of $[Cu_2(OSO_2C_6H_4Me)_2L(DMF)_2](SO_3C_6H_4Me)_2$ (compound 2) $Cu(SO_3C_6H_4Me)_2 \cdot 4H_2O \cdot CH_3OH$ (0.15 g, 0.30 mmol) and $L \cdot CH_3OH \cdot 2.5H_2O$ (0.10 g, 0.13 mmol) were dissolved in 20 mL DMF and the solution stirred for 24 h. After filtration, the filtrate was concentrated under vacuum, and 20 mL of diethyl ether was then added to give a blue solid. Different batches of the compound were used for microanalysis, TG, and single crystal X-ray diffraction. Total amount obtained: 0.21 g (79% yield based on L). Anal. calcd for $C_{68}H_{82}Cu_2N_6O_{16}S_4 \cdot 4C_3H_7NO \cdot 2H_2O$ ($C_{80}H_{114}Cu_2N_{10}O_{22}S_4$; *mw* 1823.17): C 52.70; H 6.30; N 7.68. Found: C 52.42; H 6.22; N 7.52. TG-DTA: CuO% = 10.3, weight% (for loss of H_2O and DMF) = 17.7. Calc with the formula of $C_{80}H_{114}Cu_2N_{10}O_{22}S_4$: CuO% = 8.7, weight% (for loss of H_2O and DMF) = 18.0. IR (KBr disc) (cm^{-1}): 3463 (vs), 3189 (m), 2932 (m), 1652 (vs), 1612 (m), 1513 (s, $\nu_{aryl\text{-}H}$), 1454 (m), 1386 (m), 1183 (vs), 1122 (s), 1035 (s), 1009 (s), 816 (m), 683 (s), 568 (s). UV–Vis$_{max}$ in DMF, nm (ε, $M^{-1}cm^{-1}$): 619 (39), 285 (884). Λ_M in DMF: 132 Scm^2mol^{-1}. Suitable crystals for X-ray diffraction analyses were obtained upon slow diffusion of diethyl ether into the above DMF solution of the compound.

Synthesis of $[Cu_2(ONO_2)_2L(DMF)_2](NO_3)_2$ (compound 3). The starting materials $Cu(NO_3)_2 \cdot 2.5H_2O$ (0.14 g, 0.60 mmol) and $L \cdot CH_3OH \cdot 2.5H_2O$ (0.21 g, 0.28 mmol) were mixed in 20 mL of DMF, and the system was stirred for 24 h. After filtration, slow diffusion of diethyl ether into the filtrate solution led to the formation of blue crystals, which were suitable for X-ray analysis. Different batches of the compound were used for microanalysis, TG, and single crystal X-ray diffraction. Total amount obtained: 0.17 g (49% based on L). $C_{40}H_{54}Cu_2N_{10}O_{16} \cdot 2C_3H_7NO \cdot 3.5H_2O$ ($C_{46}H_{75}Cu_2N_{12}O_{21.5}$; *mw* 1267.25): C 43.60; H 5.97; N 13.26. Found: C 43.58; H 6.21; N 13.06. TG-DTA: CuO% = 12.8, weight% (for loss of solvents) = 19.6. Calc with the formula of $C_{40}H_{54}Cu_2N_{10}O_{16} \cdot 3C_3H_7NO \cdot 3H_2O$ ($C_{49}H_{81}Cu_2N_{13}O_{22}$): CuO% = 12.0, weight% (for loss of H_2O and DMF) = 20.5. IR (KBr disc) (cm^{-1}): 3429 (vs), 3200 (m), 2933 (m), 2878 (m), 1652 (vs), 1611 (m), 1585 (s), 1513 (s, $\nu_{aryl\text{-}H}$), 1384 (vs), 1307 (m), 1248 (s), 1224 (s), 1180 (m), 1054 (m), 1031 (m), 918 (w), 826 (m), 775 (m), 693 (w), 618 (w), 518 (w). UV–Vis$_{max}$ in DMF, nm (ε, $M^{-1}cm^{-1}$): 619 (38), 282 (862). Λ_M in DMF: 166 Scm^2mol^{-1}.

Synthesis of $[Cu_2(OClO_3)_2L(DMF)_2](ClO_4)_2$ (compound 4). The starting materials $Cu(ClO_4)_2 \cdot 6H_2O$ (0.12 g, 0.32 mmol) and $L \cdot CH_3OH \cdot 2.5H_2O$ (0.10 g, 0.13 mmol), as well as 20 mL of methanol were mixed in a 50 mL flask, and the system was stirred for 24 h. After filtration, the filtrate was concentrated, and diethyl ether was added. A blue solid was obtained (0.15 g). Suitable crystals for X-ray diffraction analyses were obtained upon slow diffusion of diethyl ether into a DMF solution of the compound. (0.090 g, yield 44% based on L). Anal. calcd for $C_{40}H_{54}Cu_2Cl_4N_6O_{20} \cdot 2C_3H_7NO \cdot 4.5H_2O$ ($C_{46}H_{77}Cu_2Cl_4N_8O_{26.5}$; *mw* 1435.04): C 38.50; H 5.41; N 7.81. Found: C 38.38; H 5.38; N 7.97. IR (KBr disc) (cm^{-1}): 3438 (vs), 3240 (m), 2931 (m), 2876 (m), 1656 (vs), 1613 (m), 1513 (s, $\nu_{aryl\text{-}H}$), 1455 (m), 1415 (w), 1385 (m), 1306 (m), 1250 (s), 1226 (s), 1117 (vs), 1084 (vs), 922 (w), 834 (s), 702 (m), 626 (s). UV–Vis$_{max}$ in DMF, nm (ε, M^{-1} cm^{-1}): 618 (37), 279 (859). Λ_M in DMF: 141 Scm^2mol^{-1}.

Synthesis of $[Cu_2(OCOPh)_2L(H_2O)_2](CO_2Ph)_2$ (compound 5). The starting materials $Cu(CO_2Ph)_2$ (0.15 g, 0.50 mmol) and $L \cdot CH_3OH \cdot 2.5H_2O$ (0.17 g, 0.22 mmol) were dissolved in 20 mL of a 1:1 mixture of methanol and dichloromethane, and the system was stirred for 24 h. After filtration, the blue filtrate was taken to dryness and recrystallized from DMF and diethyl

ether to give a blue solid (0.26 g, yield 71% based on L), which was isolated by filtration and dried under vacuum. The mother solution was then mixed with 1,4-dioxane in a 2:1 ratio followed by slow evaporation, which led to the formation of X-ray quality dark blue crystals. Anal. calcd for $C_{68}H_{74}Cu_2N_6O_{12}\cdot 2C_3H_7NO\cdot 2H_2O\cdot CH_2Cl_2$ ($C_{75}H_{94}Cl_2Cu_2N_8O_{16}$; *mw* 1561.59): C 57.68; H 6.07; N 7.18. Found: C 57.97; H 6.01; N 7.05. TG-DTA: CuO% = 13.1, weight% (loss of solvents) = 6.6. Calc with the formula of $[Cu_2(CO_2Ph)_4L(H_2O)_2]\cdot 0.5DMF$ ($C_{69.5}H_{81.5}N_{6.5}O_{14.5}Cu_2$; *mw* 1367.01): CuO% = 11.6, weight% (loss of solvents) = 5.3. IR (KBr disc) (cm^{-1}): 3430 (vs), 3219 (m), 2931 (m), 2878 (m), 1665 (m), 1598 (s), 1551 (s, $\nu_{aryl\text{-}H}$), 1512 (s), 1456 (m), 1384 (vs), 1304 (w), 1244 (s), 1179 (m), 1067 (m), 1024 (w), 934 (w), 840 (m), 723 (m), 681 (w), 618 (w). UV–Vis$_{max}$ in H_2O or DCM/MeOH, nm (ε, M^{-1} cm^{-1}): 616 (45), 271 (704) and 226 (1,931), or 611 (43) and 273 (521). Λ_M in H_2O or DCM/MeOH: 226 or 131 Scm^2mol^{-1}.

Synthesis of $[Cu_2(OCOMe)_4L]$ (compound 6). The starting materials $Cu(CO_2Me)_2\cdot H_2O$ (0.059 g, 0.30 mmol) and $L\cdot CH_3OH\cdot 2.5H_2O$ (0.10 g, 0.13 mmol) were dissolved in 20 mL methanol and stirred for 2 h. After filtration, the filtrate was concentrated under vacuum, and diethyl ether was added. A dark blue solid was obtained (0.15 g). Dark blue crystals of compound **6** suitable for X-ray diffraction analyses were obtained upon dissolution of 0.10 g of the compound in 15 mL of a 2:1 mixture of methanol and 1,4-dioxane followed by slow evaporation at room temperature (0.067 g, yield 67% based on L). Anal. calcd for $C_{48}H_{66}Cu_2N_6O_{12}\cdot C_4H_8O_2\cdot 5H_2O$ ($C_{52}H_{84}Cu_2N_6O_{19}$; *mw* 1224.34): C 51.01; H 6.92; N 6.86. Found: C 50.75; H 6.96; N 6.80. TG-DTA: CuO% = 13.9, weight% (lost for solvents) = 6.9. Calc with the formula of $[Cu_2(CO_2CH_3)_4L]\cdot 0.5C_4H_{10}O_2\cdot 2.5H_2O$ ($C_{50}H_{76}Cu_2N_6O_{15.5}$; *mw* 1136.3): CuO% = 14.0, weight% (lost for the solvents) = 7.9. IR (KBr disc) (cm^{-1}): 3433 (vs), 3239 (m), 2931 (s), 2881 (m), 1614 (m), 1570 (vs), 1514 (s, $\nu_{aryl\text{-}H}$), 1409 (s), 1335 (m), 1306 (m), 1251 (s), 1181 (m), 1117 (m), 1053 (s), 985 (m), 919 (m), 869 (w), 847 (m), 767 (w), 666 (m), 618 (m); UV–Vis$_{max}$ in H_2O or DCM/MeOH, nm (ε, M^{-1} cm^{-1}): 603 (45), 270 (252) and 222 (877), or 612 (33) and 271 (527). Λ_M in H_2O or DCM/MeOH: 28 or 10 Scm^2mol^{-1}.

In 1 M K_2CO_3 aqueous solution, after 20 h at 70 °C: UV–Vis$_{max}$ in H_2O or DCM/MeOH, nm (ε, M^{-1} cm^{-1}): 606 (8), 268 (1771), and 221 (2056) or 610 (<8) and 270 (476). Λ_M in H_2O or DCM/MeOH: 248 Scm^2mol^{-1}.

4. Conclusions

Six dinuclear copper(II) complexes where both metal ions lie in the coordinating pockets of a single N_6O_4 macrocycle were synthesized and fully characterized by single-crystal X-ray diffraction. They act as catalysts for the aerobic oxidation of primary alcohols to the respective aldehydes (and also of 1-phenylethanol, as a secondary alcohol model, to acetophenone), in alkaline aqueous solution and in the presence of the TEMPO radical, as well as in solvent-free MW-assisted peroxidative (by *t*-BuOOH) oxidation of 1-phenylethanol to acetophenone. Under both reaction conditions, compound **6** is the most active catalyst with yields that reach 99% in 20 h using the former reaction settings or in just 0.5 h (TON of 542) by following the latter method. TEMPO has a marked promoting effect for both types of procedures. The use of low-power microwave irradiation and solvent-free conditions are of significance towards achieving energy-saving catalytic systems.

Supplementary Materials: The following are available online at http://www.mdpi.com/2073-4344/9/5/424/s1, **Table S1.** Decomposition processes in TG-DTA of the complexes **1-3**, **5** and **6. Figure S1-1.** A view of the crystal packing of compound **1** along the *a* axis. **Figure S1-2.** A view of the crystal packing of compound 2 along the a axis. **Figure S1-3.** A view of the crystal packing of compound 3 along the c axis. **Figure S1-4**. A view of the crystal packing of compound 4 along the a axis. **Figure S1-5**. A view of the crystal packing of compound 5 along the a axis. **Figure S1-6.** A view of the crystal packing of compound 6 along the a axis. **Figure S2-1.** Experimental and simulated EPR spectra of a DMF solution of **1**. **Figure S2-2**. Experimental and simulated EPR spectra of a DMF solution of 2. **Figure S2-3.** Experimental and simulated EPR spectra of a DMF solution of 3. **Figure S2-4**. Experimental and simulated EPR spectra of a dichloromethane:methanol (0.85:0.15) solution of 5. **Figure S2-5**. Experimental and simulated EPR spectra of a dichloromethane:methanol (0.85:0.15) solution of 6**. Figure S3-1**. TG-DTA curves of compound 1. **Figure S3-2**. TG-DTA curves of compound 2. **Figure S3-3**. TG-DTA curves of compound 3. **Figure S3-4.** TG-DTA curves of compound 5. **Figure S3-5**. TG-DTA curves of compound 6.

Author Contributions: Z.M. conceived and designed the experiments; Z.M. and Q.W. prepared the N_6O_4 macrocycles and compounds **1-6**. Z.M. and M.F.C.G.d.S. performed, solved and discussed the single-crystal X-ray diffraction data; J.P.T. and I.C. performed, analysed and discussed EPR data; L.M.D.R.S.M. performed and discussed the electrochemical studies, E.C.B.A.A. performed and discussed the catalytic experiments; Z.M., M.F.C.G.d.S. and A.J.L.P. discussed the whole data and wrote the paper. All authors read and approved the manuscript.

Funding: This research was funded by the Science Foundation of China (21261002) and the Fundação para a Ciência e a Tecnologia (FCT), Portugal (projects UID/QUI/00100/2019 and PTDC/QEQ-QIN/3967/2014). Z.M. gratefully acknowledges FCT grant SFRH/BPD/24691/2005 and I.C. thanks the programme Investigador FCT.

Conflicts of Interest: The authors declare no conflicts of interest.

References

1. Amouri, H.; Desmarets, C.; Moussa, J. Confined Nanospaces in Metallocages: Guest Molecules, Weakly Encapsulated Anions, and Catalyst Sequestration. *Chem. Rev.* **2012**, *112*, 2015–2041. [CrossRef]
2. Alibrandi, G.; Arena, C.G.; Lando, G.; Vecchio, C.L.; Parisi, M.F. {[1.1.1]Cryptand/Imidazole}: A Prototype Composite Kinetic Molecular Device for Automatic NMR Variable pH Reaction Monitoring. *Chem. Eur. J.* **2011**, *17*, 1419–1422. [CrossRef] [PubMed]
3. Garcia, J.; Kuda-Wedagedara, A.N.W.; Allen, M.J. Physical Properties of Eu^{2+}-Containing Cryptates as Contrast Agents for Ultrahigh-Field Magnetic Resonance Imaging. *Eur. J. Inorg. Chem.* **2012**, *2012*, 2135–2140. [CrossRef] [PubMed]
4. Nelson, J.; Mckee, V.; Morgan, G. Coordination Chemistry of Azacryptands. *Prog. Inorg. Chem.* **2007**, *47*, 167–317.
5. Geoghegan, P.; O' Leary, P. Hydroxyamide-Based Ligands and Their Use in the Asymmetric Catalysis of Key Organic Transformations. *ACS Catal.* **2012**, *2*, 573–591. [CrossRef]
6. Mateus, P.; Delgado, R.; Brandão, P.; Félix, V. Dicarboxylate Recognition by Two Macrobicyclic Receptors: Selectivity for Fumarate over Maleate. *J. Org. Chem.* **2012**, *77*, 4611–4621. [CrossRef]
7. Zhu, K.; Wu, L.; Yan, X.; Zheng, B.; Zhang, M.; Huang, F. Anion-Assisted Complexation of Paraquat by Cryptands Based on Bis(*m*-phenylene)-[32]crown-10. *Chem. Eur. J.* **2010**, *16*, 6088–6098. [CrossRef]
8. Alibrandi, G.; Vecchio, C.L.; Lando, G. [1.1.1]Cryptand: A Molecular Automatic Titrator. *Angew. Chem. Int. Ed.* **2009**, *48*, 6332–6334. [CrossRef]
9. Xu, Z.; Huang, X.; Liang, J.; Zhang, S.; Zhou, S.; Chen, M.; Tang, M.; Jiang, L. Efficient Syntheses of Novel Cryptands Based on Bis(*m*-phenylene)-26-crown-8 and Their Complexation with Paraquat. *Eur. J. Org. Chem.* **2010**, *2010*, 1904–1911. [CrossRef]
10. Gamage, N.H.; Mei, Y.; Garcia, J.; Allen, M.J. Oxidatively Stable, Aqueous Europium(II) Complexes through Steric and Electronic Manipulation of Cryptand Coordination Chemistry. *Angew. Chem. Int. Ed.* **2010**, *49*, 8923–8925. [CrossRef] [PubMed]
11. Chaloner, L.; Askari, M.S.; Kutteh, A.; Schindler, S.; Ottenwaelder, X. Formation and Reactivity of a Biomimetic Hydroperoxocopper(II) Cryptate. *Eur. J. Inorg. Chem.* **2011**, *2011*, 4204–4211. [CrossRef]
12. Liu, M.; Li, S.; Hu, M.; Wang, F.; Huang, F. Selectivity Algorithm for the Formation of Two Cryptand/Paraquat Catenanes. *Org. Lett.* **2010**, *12*, 760–763. [CrossRef]
13. Hao, H.G.; Zheng, X.D.; Lu, T.B. Photoinduced Catalytic Reaction by a Fluorescent Active Cryptand Containing an Anthracene Fragment. *Angew. Chem. Int. Ed.* **2010**, *49*, 8148–8151. [CrossRef]
14. Alliger, G.E.; Müller, P.; Do, L.H.; Cummins, C.C.; Nocera, D.G. Family of Cofacial Bimetallic Complexes of a Hexaanionic Carboxamide Cryptand. *Inorg. Chem.* **2011**, *50*, 4107–4115. [CrossRef]
15. Cangelosi, V.M.; Carter, T.G.; Crossland, J.L.; Zakharov, L.N.; Johnson, D.W. Self-Assembled E2L3 Cryptands (E = P, As, Sb, Bi): Transmetalation, Homo- and Heterometallic Assemblies, and Conformational Isomerism. *Inorg. Chem.* **2010**, *49*, 9985–9992. [CrossRef]
16. Yan, X.; Wei, P.; Zhang, M.; Chi, X.; Liu, J.; Huang, F. [2]Pseudorotaxanes Based on the Recognition of Cryptands to Vinylogous Viologens. *Org. Lett.* **2011**, *13*, 6370–6373. [CrossRef]
17. Saeed, M.A.; Wong, B.M.; Fronczek, F.R.; Venkatraman, R.; Hossain, M.A. Formation of an Amine-Water Cyclic Pentamer: A New Type of Water Cluster in a Polyazacryptand. *Cryst. Growth Des.* **2010**, *10*, 1486–1488. [CrossRef]
18. Ma, Z.; Cao, R. An N_8O_6 cryptand: The host for Ag^+ guests and H_2O molecule. *J. Mol. Struct.* **2005**, *738*, 137–142. [CrossRef]

19. Alliger, G.E.; Müller, P.; Cummins, C.C.; Nocera, D.G. Cofacial Dicobalt Complex of a Binucleating Hexacarboxamide Cryptand Ligand. *Inorg. Chem.* **2010**, *49*, 3697–3699. [CrossRef]
20. Bischof, C.; Wahsner, J.; Scholten, J.; Trosien, S.; Seitz, M. Quantification of C−H Quenching in Near-IR Luminescent Ytterbium and Neodymium Cryptates. *J. Am. Chem. Soc.* **2010**, *132*, 14334–14335. [CrossRef]
21. Cangelosi, V.M.; Zakharov, L.N.; Johnson, D.W. Supramolecular "Transmetalation" Leads to an Unusual Self-Assembled P_2L_3 Cryptand. *Angew. Chem. Int. Ed.* **2010**, *49*, 1248–1251. [CrossRef] [PubMed]
22. Yoshida, A.; Nakagawa, Y.; Uehara, K.; Hikichi, S.; Mizuno, N. Inorganic Cryptand: Size-Selective Strong Metallic Cation Encapsulation by a Disilicoicosatungstate (Si_2W_{20}) Polyoxometalate. *Angew. Chem. Int. Ed.* **2009**, *48*, 7055–7058. [CrossRef] [PubMed]
23. Shen, Z.; Jordan, R.F. Self-Assembled Tetranuclear Palladium Catalysts That Produce High Molecular Weight Linear Polyethylene. *J. Am. Chem. Soc.* **2010**, *132*, 52–53. [CrossRef] [PubMed]
24. Mateus, P.; Delgado, R.; Brandão, P.; Félix, V. Recognition of Oxalate by a Copper(II) Polyaza Macrobicyclic Complex. *Chem. Eur. J.* **2011**, *17*, 7020–7031. [CrossRef] [PubMed]
25. Hossain, M.A.; Saeed, M.A.; Fronczek, F.R.; Wong, B.M.; Dey, K.R.; Mendy, J.S.; Gibson, D. Charge-Assisted Encapsulation of Two Chlorides by a Hexaprotonated Azamacrocycle. *Cryst. Growth Des.* **2010**, *10*, 1478–1481. [CrossRef] [PubMed]
26. Ma, Z.; Shi, H.; Deng, X.; Guedes da Silva, M.F.C.; Martins, L.M.D.R.S.; Pombeiro, A.J.L. Silver coordination polymers with tri- and hexacyanoethyl-functionalized macrocyclic ligands. *Dalton Trans.* **2015**, *44*, 1388–1396. [CrossRef]
27. Ghosh, M.; Weyhermuller, T.; Wieghardt, K. Electronic structure of the members of the electron transfer series $[NiL]^z$ (z = 3+, 2+, 1+, 0) and $[NiL(X)]^n$ (X = Cl, CO, $P(OCH_3)_3$) species containing a tetradentate, redox-noninnocent, Schiff base macrocyclic ligand L: An experimental and density functional theoretical study. *Dalton Trans.* **2010**, *39*, 1996–2007. [PubMed]
28. Gamez, P.; Aubel, P.G.; Driessen, W.L.; Reedijk, J. Homogeneous bio-inspired copper-catalyzed oxidation reactions. *Chem. Soc. Rev.* **2001**, *30*, 376–385. [CrossRef]
29. Ma, Z.; Zhang, B.; Guedes da Silva, M.F.C.; Silva, J.; Mendo, A.S.; Baptista, P.V.; Fernandes, A.R.; Pombeiro, A.J.L. Synthesis, characterization, thermal properties and antiproliferative potential of copper(II) 4′-phenylterpyridine compounds. *Dalton Trans.* **2016**, *45*, 5339–5355. [CrossRef]
30. Lewis, E.A.; Tolman, W.B. Reactivity of Dioxygen−Copper Systems. *Chem. Rev.* **2004**, *104*, 1047–1076. [CrossRef]
31. Itoh, S. *Comprehensive Coordination Chemistry*, 2nd ed.; McCleverty, J.A., Meyer, T.J., Eds.; Elsevier: Amsterdam, The Netherlands, 2003; Volume 8, Chapter 8.15, p. 369.
32. Lee, D.H. *Comprehensive Coordination Chemistry*, 2nd ed.; McCleverty, J.A., Meyer, T.J., Eds.; Elsevier: Amsterdam, The Netherlands, 2003; Volume 8, Chapter 8.17, p. 437.
33. Fraústo da Silva, J.J.R.; Williams, R.J.P. *The Biological Chemistry of the Elements*; Oxford University Press: Oxford, UK, 2001.
34. Solomon, E.I.; Sundaram, U.M.; Machonkin, T.E. Multicopper Oxidases and Oxygenases. *Chem. Rev.* **1996**, *96*, 2563–2606. [CrossRef] [PubMed]
35. Klinman, J.P. Mechanisms Whereby Mononuclear Copper Proteins Functionalize Organic Substrates. *Chem. Rev.* **1996**, *96*, 2541–2562. [CrossRef]
36. Ayala, M.; Torres, E. Enzymatic activation of alkanes: Constraints and prospective. *Appl. Catal. A Gen.* **2004**, *272*, 1–13. [CrossRef]
37. Elliot, S.J.; Zhu, M.; Tso, L.; Nguyen, H.-H.T.; Yip, J.H.-K.; Chan, S.I. Regio- and Stereoselectivity of Particulate Methane Monooxygenase from *Methylococcus capsulatus* (Bath). *J. Am. Chem. Soc.* **1997**, *119*, 9949–9955. [CrossRef]
38. Lieberman, R.L.; Rosenzweig, A.C. Biological methane oxidation: Regulation, biochemistry, and active site structure of particulate methane monooxygenase. *Crit. Rev. Biochem. Mol. Biol.* **2004**, *39*, 147–164. [CrossRef]
39. Lieberman, R.L.; Rosenzweig, A.C. Crystal structure of a membrane-bound metalloenzyme that catalyses the biological oxidation of methane. *Nature* **2005**, *434*, 177–182. [CrossRef]
40. Kopylovich, M.N.; Ribeiro, A.P.C.; Alegria, E.C.B.A.; Martins, N.M.R.; Martins, L.M.D.R.S.; Pombeiro, A.J.L. Catalytic oxidation of alcohols: Recent advances. *Adv. Organometal. Chem.* **2015**, *63*, 91–174.
41. Pombeiro, A.J.L.; Guedes da Silva, M.F.C.; Lemos, M.A.N.D.A. Electron-Transfer Induced Isomerizations of Coordination Compounds. *Coord. Chem. Rev.* **2001**, *219*, 53–80. [CrossRef]

42. Addison, A.W.; Rao, T.N.; Reedijk, J.; van Rijn, J.; Verschoor, G.C. Synthesis, structure, and spectroscopic properties of copper(II) compounds containing nitrogen–sulphur donor ligands; the crystal and molecular structure of aqua[1,7-bis(N-methylbenzimidazol-2-yl)-2,6-dithiaheptane]copper(II) perchlorate. *J. Chem. Soc. Dalton Trans.* **1984**, 1349–1356. [CrossRef]
43. Di Nicola, C.; Garau, F.; Karabach, Y.Y.; Martins, L.M.D.R.S.; Monari, M.; Pandolfo, L.; Pettinari, C.; Pombeiro, A.J.L. Trinuclear Triangular Copper(II) Clusters-Synthesis, Electrochemical Studies and Catalytic Peroxidative Oxidation of Cycloalkanes. *Eur. J. Inorg. Chem.* **2009**, *2009*, 666–676. [CrossRef]
44. Lewis, W.B.; Alei, M., Jr.; Morgan, L.O. Magnetic resonance studies on copper(II) complex ions in solution. I. Temperature dependences of the ^{17}O NMR and copper(II) EPR linewidths of $Cu(H_2O)_6^{2+}$. *J. Chem. Phys.* **1966**, *44*, 2409–2417. [CrossRef]
45. Sakaguchi, U.; Addison, A.W. Spectroscopic and redox studies of some copper(II) complexes with biomimetic donor atoms: Implications for protein copper centres. *J. Chem. Soc. Dalton Trans.* **1979**, *1979*, 600–608. [CrossRef]
46. Kopylovich, M.N.; Mahmudov, K.T.; Guedes da Silva, M.F.C.; Kuznetsov, M.L.; Figiel, P.J.; Karabach, Y.Y.; Luzyanin, K.V.; Pombeiro, A.J.L. *Ortho*-hydroxyphenylhydrazo-β-diketones: Tautomery, Coordination Ability and Catalytic Activity of Their Copper(II) Complexes toward Oxidation of Cyclohexane and Benzylic Alcohols. *Inorg. Chem.* **2011**, *50*, 918–931. [CrossRef]
47. Sheldon, R.A.; Arends, I.W.C.E. Organocatalytic Oxidations Mediated by Nitroxyl Radicals. *Adv. Synth. Catal.* **2004**, *346*, 1051–1071. [CrossRef]
48. de Mico, A.; Margarita, R.; Mariani, A.; Piancatelli, G. Radical additions to olefins in the presence of iodobenzenediacetate: An easy route to alkyl dithiocyanates. *Tetrahedron Lett.* **1996**, *37*, 1889–1892. [CrossRef]
49. Dijksman, A.; Arends, I.W.C.E.; Sheldon, R.A. The ruthenium/TEMPO-catalysed aerobic oxidation of alcohols. *Platin. Metals Rev.* **2001**, *45*, 15–19.
50. Mahmudov, K.T.; Kopylovich, M.N.; Guedes da Silva, M.F.C.; Figiel, P.J.; Karabach, Y.Y.; Pombeiro, A.J.L. New copper(II) dimer with 3-(2-hydroxy-4-nitro-phenylhydrazo)pentane-2,4-dione and its catalytic activity in cyclohexane and benzyl alcohol oxidations. *J. Mol. Catal. A Chem.* **2010**, *318*, 44–50. [CrossRef]
51. Soroceanu, A.; Cazacu, M.; Shova, S.; Turta, C.; Kožíšek, J.; Gall, M.; Breza, M.; Rapta, P.; Mac Leod, T.C.O.; Pombeiro, A.J.L.; et al. Copper(II) Complexes with Schiff Bases Containing a Disiloxane Unit: Synthesis, Structure, Bonding Features and Catalytic Activity for Aerobic Oxidation of Benzyl Alcohol. *Eur. J. Inorg. Chem.* **2013**, *2013*, 1458–1474. [CrossRef]
52. Arends, I.W.C.A.; Sheldon, R.A. *Modern Oxidation Methods*; Bäckvall, J.-E., Ed.; Wiley: Weinheim, Germany, 2004; p. 83.
53. Michel, C.; Belanzoni, P.; Gamez, P.; Reedijk, J.; Baerends, E.J. Activation of the C−H Bond by Electrophilic Attack: Theoretical Study of the Reaction Mechanism of the Aerobic Oxidation of Alcohols to Aldehydes by the $Cu(bipy)^{2+}$/2,2,6,6-Tetramethylpiperidinyl-1-oxy Cocatalyst System. *Inorg. Chem.* **2009**, *48*, 11909–11920. [CrossRef]
54. Sutradhar, M.; Martins, L.M.D.R.S.; Guedes da Silva, M.F.C.; Alegria, E.C.B.A.; Liu, C.-M.; Pombeiro, A.J.L. Dinuclear Mn(II,II) complexes: Magnetic properties and microwave assisted oxidation of alcohols. *Dalton Trans.* **2014**, *43*, 3966–3977. [CrossRef]
55. Arion, V.B.; Platzer, S.; Rapta, P.; Machata, P.; Breza, M.; Vegh, D.; Dunsch, L.; Telser, J.; Shova, S.; Mac Leod, T.C.O.; et al. Marked stabilization of redox states and enhanced catalytic activity in galactose oxidase models based on transition metal S-methylisothiosemicarbazonates with –SR group in ortho-position to the phenolic oxygen. *Inorg. Chem.* **2013**, *52*, 7524–7540. [CrossRef]
56. Sabbatini, A.; Martins, L.M.D.R.S.; Mahmudov, K.T.; Kopylovich, M.N.; Drew, M.G.B.; Pettinari, C.; Pombeiro, A.J.L. Microwave-assisted and solvent-free peroxidative oxidation of 1-phenylethanol to acetophenone with a Cu^{II}–TEMPO catalytic system. *Catal. Commun.* **2014**, *48*, 69–72. [CrossRef]
57. Sheldon, R.A. E factors, green chemistry and catalysis: An odyssey. *Chem. Commun.* **2008**, *29*, 3352–3365. [CrossRef]
58. Sutradhar, M.; Alegria, E.C.B.A.; Mahmudov, K.T.; Guedes da Silva, M.F.C.; Pombeiro, A.J.L. Iron(III) and cobalt(III) complexes with both tautomeric (keto and enol) forms of aroylhydrazone ligands: Catalysts for the microwave assisted oxidation of alcohols. *RSC Adv.* **2016**, *6*, 8079–8088. [CrossRef]

59. Dronova, M.S.; Bilyachenko, A.N.; Yalymov, A.I.; Kozlov, Y.N.; Shul'pina, L.S.; Korlyukov, A.A.; Arkhipov, D.E.; Levitsky, M.M.; Shubina, E.S.; Shul'pin, G.B. Solvent-controlled synthesis of tetranuclear cage-like copper(II) silsesquioxanes. Remarkable features of the cage structures and their high catalytic activity in oxidation with peroxides. *Dalton Trans.* **2014**, *43*, 872–882. [CrossRef]
60. Sutradhar, M.; Martins, L.M.D.R.S.; Carabineiro, S.A.C.; Guedes da Silva, M.F.C.; Buijnsters, J.G.; Figueiredo, J.L.; Pombeiro, A.J.L. Oxidovanadium(V) complexes anchored on carbon materials as catalysts for the oxidation of 1-phenylethanol. *ChemCatChem* **2016**, *8*, 2254–2266. [CrossRef]
61. Rockenbauer, A.; Korecz, L. Automatic computer simulations of ESR spectra. *Appl. Magn. Reson.* **1996**, *10*, 29–43. [CrossRef]
62. *CrysAlisPRO*, version 171.36.20; Oxford Diffraction/Agilent Technologies UK Ltd.: Yarnton, Oxfordshire, UK, 2011.
63. Bruker. *APEX2*; Bruker AXS Inc.: Madison, WI, USA, 2012.
64. Sheldrick, G.M. *SADABS. Program for Empirical Absorption Correction*; University of Gottingen: Gottingen, Germany, 1996.
65. Sheldrick, G.M. *SHELX97. Programs for Crystal Structure Analysis (Release 97-2)*; University of Göttingen: Göttingen, Germany, 1997.
66. Farrugia, L.J. WinGX suite for small-molecule single-crystal crystallography. *J. Appl. Crystallogr.* **1999**, *32*, 837–838. [CrossRef]
67. Guedes da Silva, M.F.C.; Pombeiro, A.J.L. Redox Potential Parameterization in Coordination Compounds with Polydentate Scorpionate and Benzene Ligands. *Electrochim. Acta* **2012**, *82*, 478–483. [CrossRef]
68. Ma, Z.; Liu, S.-X. Synthesis and Characterization of a Macrocyclic Compound, $C_{40}H_{46}N_6O_4$. *Chin. J. Struct. Chem.* **2003**, *22*, 553–557.